IMPURITIES IN METALS AND SUPERCONDUCTORS

By

MATTHIAS H. HETTLER

A DISSERTATION PRESENTED TO THE GRADUATE SCHOOL
OF THE UNIVERSITY OF FLORIDA IN PARTIAL FULFILLMENT
OF THE REQUIREMENTS FOR THE DEGREE OF
DOCTOR OF PHILOSOPHY

UNIVERSITY OF FLORIDA

1996

ACKNOWLEDGMENTS

It is my pleasure to thank Professor Peter J. Hirschfeld for his guidance, encouragement and patience for last four years. I feel myself very fortunate not only to have benefited from his academic guidance but also to have enjoyed his invaluable friendship.

Special thanks also to Professor Selman Hershfield who taught me many things and who was advising on most of the first part of this thesis.

I also thank Professors Klauder, Muttalib, Simmons and Tanner for their academic advice and for serving on my supervisory committee.

In addition, my gratitude goes to my fellow graduate students who have been good friends throughout these years, in random order, Carsten and Andrea, Wolfgang and Jacqueline, Dmitry and Elena, Mirim and Jae Wan, Bruce, Jianzhong, Anatoly, Allison, Mark, Kiho, Gwyneth and Samuel.

I am very grateful to my family in Germany, especially my parents. I can not thank them enough. Their love and support made it possible for me to accomplish what I have.

Finally, I want to express my deep gratitude to my best friend and wife Namkyoung Lee, for her encouragement, support and understanding.

TABLE OF CONTENTS

Abstract of Dissertation Presented to the Graduate School
of the University of Florida in Partial Fulfillment of the
Requirements for the Degree of Doctor of Philosophy

IMPURITIES IN METALS AND SUPERCONDUCTORS

By

Matthias H. Hettler

December 1996

Chairman: Peter J. Hirschfeld
Major Department: Physics

This thesis deals with transport properties like conductance or conductivity of systems in which a small concentration of impurities has been added to an otherwise pure material. The small number of impurities implies that the distance between impurities is large enough to neglect direct interactions between the impurities. Therefore, all the physics is a result of the interaction of the host material with a single impurity. Depending on the nature of the host and the nature of the impurity, the physics changes qualitatively or merely quantitatively. Under qualitative changes I understand a change in the functional, often power–law dependence of physical properties on variables like the temperature. Quantitative changes imply only changes in certain constants, leaving the functional dependence unaffected.

I will discuss two systems in which qualitative changes in transport proper-

ties occur. In the first case, this is due to the special nature of the impurity. I consider the effects of a nonmagnetic impurity with two states of equal energy on the conductance of clean metal point contacts and metal–insulator–metal tunnel junctions. At low temperatures, the conductance shows a power–law dependence on temperature and applied voltage different from the system without the impurity. Such behavior has been observed in experiments. I will show that the experimental and theoretical results are in reasonable agreement.

The second part of the thesis deals with nonmagnetic impurities in a "d–wave" superconductor, a system probably closely related the "high–T_c" superconductors. In this case, it is the"exotic" host materials which leads to effects not anticipated from their "classic" counterparts. Again, the interplay of host and impurity leads to qualitative changes in the transport properties. The new effects might help to understand a puzzle of the low temperature properties of the high-T_c materials, for which the standard model (which can qualitatively explain the thermodynamic properties like specific heat) fails to reproduce the experimentally observed power–laws of the transport properties.

CHAPTER 1
INTRODUCTION

Crystalline solid state materials can be divided into two classes: pure materials and materials with impurities. A pure material is usually a lattice of one or more species of atoms. Every deviation from the perfect lattice structure is considered an impurity. Examples are interstitional atoms, dislocations and substitution of some atoms by others not present in the perfect stochiometry. If the concentration of impurities is large, one approaches the amorphous state, where the long range cristalline order is severely perturbed. I will not consider such systems.

I do consider materials with small amounts of impurities such that the distance between impurities is large enough to neglect direct interactions between impurities. In this case, the physics is determined by the interaction of the host material with a single impurity. Depending on the nature of the host and the impurity, the physics can change qualitatively or merely quantitatively. Often, some physical properties are rather inert to small amounts of impurities, whereas transport properties like conductance or conductivity are rather sensitive and show qualitative different behavior in the pure and impure systems.

In the first part of this thesis I consider the effects of impurities of a special type on the transport properties of clean metal point contacts and metal–insulator–metal tunnel junctions. At low temperatures, due to the nature of the impurity, the conductance shows dramatically different behavior compared to

the pure system. Such behavior has been observed in experiments by Ralph and Buhrman in 1992 [1].

The second part of the thesis deals with standard, nonmagnetic impurities in an anisotropic, "d–wave" superconductor, probably close relatives to the ceramic, high–T_c superconductors discovered by Bednorz and Müller in 1986 [2]. In this case, it is the"exotic" host materials which leads to effects not anticipated from their "classic" counterparts, the metallic superconductors first observed by Onnes in 1911 [3]. The new effects might help to understand the puzzle of low temperature transport properties.

CHAPTER 2
PART I: ANDERSON IMPURITIES IN POINT CONTACTS AND TUNNEL JUNCTIONS

Anderson [4] introduced a model describing a conduction band of electrons hybridizing with a localized, N–fold degenerate impurity level with on–site interaction.

$$\begin{aligned} H = & \sum_{p,\sigma}(\epsilon_p - \mu)c^\dagger_{p\sigma}c_{p\sigma} + \epsilon_d \sum_{\sigma} d^\dagger_\sigma d_\sigma + U d^\dagger_\sigma d_\sigma d^\dagger_{-\sigma} d_{-\sigma} \\ & + \sum_{p,\sigma} W(d^\dagger_\sigma c_{p\sigma} + h.c.) \end{aligned} \tag{2.1}$$

This was a step beyond the s–d exchange model introduced by Zener [5] which described conduction electrons interaction with a dilute concentration of localized magnetic moments. The Anderson model allows the study of how such localized moments are formed. It is more physical and has much richer behavior, due to the interplay of the energy scales ϵ_d, U and $\Gamma = \pi N_o W^2$ (N_o is the density of conduction electron states at the Fermi level). In particular, it can be shown via a Schrieffer–Wolff [6] transformation, that in the limit $U = -2\epsilon_d \to \infty, W \to \infty$ such that $\Gamma/\epsilon_d = N_o J$ is kept constant, the model maps onto the s–d model with an antiferromagnetic exchange coupling $J = W^2/\epsilon_d$.

$$H = \sum_{p,\sigma}(\epsilon_p - \mu)c^\dagger_{p\sigma}c_{p\sigma} - J\vec{S} \sum_{p,p',\alpha,\beta} c^\dagger_{p\alpha}\vec{\sigma}_{\alpha\beta}c_{p\beta} \tag{2.2}$$

If one lets U and $-\epsilon_d$ independently go to infinity, one also creates a potential scattering term due to the lack of particle–hole symmetry. For a wide conduction band that is flat about the Fermi level, this potential scattering terms are unimportant for the low temperature physics. However, they can play important roles for systems with bands of vanishing DOS at the Fermi level [7].

In the following I will show how the formation of local magnetic moments and their interaction with the conduction electrons as described by the s–d model can be understood by looking at scattering processes of the electrons off the Anderson impurity. I will then summarize the physics involved in the screening of these magnetic moments at low temperatures, widely known under the term "Kondo effect" [8]. To obtain dynamic properties I will use a self–consistent approximation technique known as "Noncrossing Approximation" (NCA) [9–12]. The NCA can be formulated for both equilibrium and nonequilibrium situations and is especially suitable for the two–channel Anderson model [13] in which there are two species of conduction electrons interacting with the Anderson impurities.

I will discuss how transport properties like the nonlinear conductance can be calculated for a tunnel junction with an Anderson impurity in the insulating layer separating the metallic leads. Similar expression can be obtained for clean point contacts. Within the NCA I compute the nonlinear conductance and show that there is scaling to leading order for temperatures and applied bias well below the characteristic energy scale of the system, the Kondo temperature T_K. This behavior is in quantitative agreement with experiments on clean metal point contacts by Ralph and Buhrmann [1, 14], if one assumes the presence of

two–channel Anderson impurities in the narrow region which defines the point contact. Finally, I also discuss the effect of a finite bias on the dynamic and static susceptibility for a two–channel Anderson model. This part of the thesis will be then summarized in the conclusions.

CHAPTER 3
LOCAL MOMENT FORMATION AND THE KONDO EFFECT

In this chapter I discuss how the formation of local magnetic moments and their interactions with the conduction electrons can be understood within the Anderson model, described by the hamiltonian Eq. 2.1. I will then summarize the screening of the local moments at low temperatures, known as the Kondo effect. I will also generalize to the multichannel Kondo model [13] and describe qualitatitive differences of the single and two channel Kondo models.

3.1 Formation of Local Magnetic Moments

The Anderson hamiltonian Eq. 2.1 describes two subsystems interacting with each other. The noninteracting conduction electrons (described by the operators $c^\dagger, c$) are characterized by a wide band of bandwidth D and a Fermi energy ϵ_F. I assume that the DOS $N(\omega)$ of these electrons is flat around the Fermi levels for the energies of interest which are either the temperature T or the characteristic energy of the Kondo effect, the Kondo temperature T_K. For convenience, I measure all energies from the Fermi level, that is I take $\epsilon_F = 0$.

The local level has two energy scales: The energy of a singly occupied level ϵ_d and the interaction energy of electrons on the local level U. I will mainly consider the case of a two–fold degenerate leve, that is $N = 2$. There are 4 different states of the local level, depending on its occupation.

- The empty level, Fig. 3.1 a). All energies are in the conduction band. The energy of this state is zero (since $\epsilon_F = 0$).
- The singly occupied states, Fig. 3.1 b). Since I assume degeneracy, the level has the same energy when occupied by either a spin up or spin down electron, namely ϵ_d.
- The doubly occupied state. Fig. 3.1 c). Due to the Pauli principle, the only possible doubly occupied state is a state with both a spin–up and a spin–down on the level. The energy of this state is $2\epsilon_d + U$.

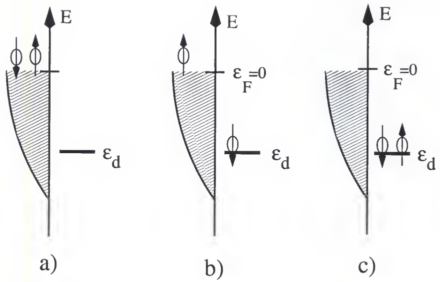

Figure 3.1: States of an Anderson impurity. a) The empty state has no electron on the impurity, all particles are in the conduction band, indicated by the shaded area. b) The singly occupied state has a single electron on the impurity site. In the figure, an electron with spin down occupies the site. The state with an up–spin on the site has identical energy (in zero magnetic field). c) The doubly occupied state has two electrons on the impurity site. Due to the Pauli principle, the electrons must have opposite spin.

The energy U is usually large and positive because it is an effective Coulomb repulsion of the electrons on the local level. Therefore, double occupancy is unlikely, unless ϵ_d is negative and $|\epsilon_d| > U$. In the following I will assume $|\epsilon_d| \leq U/2$.

The occupancy of the local level is now determined by the size and sign of ϵ_d. I can distinguish three regimes:

- The empty impurity limit, $\epsilon_d >> 0$. If ϵ_d is large and positive, the impurity level will be essentially empty, the occupancy is close to zero.

- The mixed valence regime, $|\epsilon_d| \sim 0$. Since $\epsilon_d \sim \epsilon_F$, electrons can be in the band as well as on the impurity without increasing their energy. The occupancy will be about 1/2.

- The Kondo limit, $|\epsilon_d| > \Gamma = \pi N_o W^2$. If ϵ_d is negative and but larger in magnitude than the inverse lifetime of the singly occupied state, the level is singly occupied essentially all the time and the occupancy is close to unity.

It is in the Kondo limit where the immediate interest lies. To see that in this case the local level behaves like a local magnetic moment, consider the second order process of exchanging a spin–up by a spin–down electron on the level, Fig. 3.2.

In Fig. 3.2 a) the level is occupied by a spin–down electron. To empty the level, one has to use the hybridization matrix element W, the electron has to go to the Fermi level, Fig. 3.2 b). The local level is now empty and can be occupied by either spin–up or spin–down electron. The former would restore the original state

and the process would be ordinary (nonmagnetic) scattering. In the latter case, a spin–up electron from the Fermi level (due to energy conservation) occupies the local level, again by use of the hybridization matrix element W. The end result is Fig. 3.2 c), an exchange of spins on the local level (with an opposite change in the Fermi sea). Thus, this second order process within the Anderson model is very similar to the (first order) spin flip process of a local magnetic moment of the Kondo model. The energy J associated with this spin flip is $J = W^2/\epsilon_d$, where the denominator comes from the energy difference of of the initial (final) state and the (virtual) intermediate state. Observe that in the Kondo limit J is negative, corresponding to antiferromagnetic coupling of the electrons to the local moment.

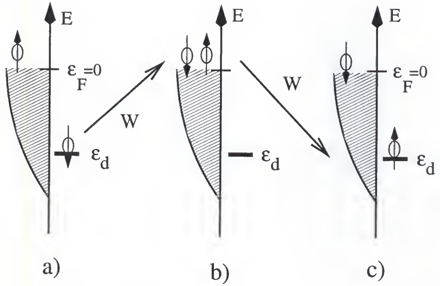

Figure 3.2: Spin–flip process in an Anderson model

In a similar process, I could have first let the spin–down electron hop on the local level, thus creating a doubly occupied level, before the spin–up electron

hops into the Fermi sea. This process creates a coupling $J_U = -W^2/(\epsilon_d + U)$. In this thesis I will only consider the limit of large U, $U >> |\epsilon_d|$. This leads to $|J_U| << |J|$, so I can neglect the processes involving doubly occupied states.

The above processes are only important when the local level is indeed occupied. This is the case in the Kondo limit, where ϵ_d is large and negative. However, if I let $|\epsilon_d|$ grow, the coupling $J = W^2/\epsilon_d$ will become small. The mapping of the Anderson model is achieved by scaling the energies W and ϵ_d so that $J = W^2/\epsilon_d$ remains constant. In the special case $\epsilon_d = -U/2 \to \infty$, one obtains the Kondo model, i.e. the hamiltonian Eq. 2.2. If I let first $U \to \infty$ and then $\epsilon_d \to -\infty$, I have broken particle–hole symmetry already in the Anderson model, which translates to additional potential scattering in the corresponding Kondo model. For the flat density of states $N(\omega)$ of the band electrons I consider, these potential scattering terms do not change the qualitative physics at low temperatures.

3.2 The Kondo Effect

The Kondo effect is one of the most fascinating examples of many–body effects, probably only topped by superconductivity. There are many books and reviews about various aspects of it. The fundamental problem of treating an inherently strongly interacting system has motivated many new techniques, of which the Numerical Renormalization Group (NRG) developed by Wilson [15,16] has been the first to give essentially exact statements [17–22] about the low temperature physics of the problem.

Kondo [8] computed the self energy of the Kondo model Eq. 2.2 within third–

order perturbation theory. Completely unexpectedly, he found a logarithmic divergence of the third order contribution at low temperatures. The logarithmic contribution immediately explained the resistivity minimum observed in certain rare earth alloys and the logarithmic upturn of the resistivity at temperatures below the minimum. However, the result also implied that straightforward perturbation theory would fail at very low temperatures, since logarithmic contributions were shown to occur also at higher order terms, invalidating any theory which would account only for a finite number of diagrams. Abrikosov [23] attempted to sum up the leading order logarithmic divergences. He found an expression for the self energy with a divergence at a finite temperature $\sim T_K$. It became obvious that nonperturbative methods had to be employed in order to get definite answers for the low temperature regime.

One approach was the poor man's renormalization group developed by Anderson and Yuval [24], which reinterpreted the problems of perturbation theory as a problem of a increasing coupling constant $J(T)$. They showed that although the bare coupling J can be small at high (room) temperature, renormalization effects lead to a strong, at first logarithmic increase of J at low temperatures. J increases until it becomes too large for the system to be reasonably described by perturbation theory. Finally, in a ground breaking work, Wilson employed his NRG to the Kondo model [15]. He showed that J indeed increases over any bounds as the temperature is lowered. This implies a formation of many–body bound state of the impurity spins with the surrounding electrons. Due to the antiferromagneticity of the coupling, this bound state is a singlet. For an elec-

tron far away from the impurity, the magnetic moment is perfectly screened. Therefore, it becomes conceivable that the low temperature state of the system is actually a Fermi liquid, i.e. a system of weakly interacting fermions. The weak interaction comes from the polarization of the screening cloud in the presence of additional electrons.

Depending on the temperature, the system is in one of three regimes which are not separated by phase transitions but have smooth crossovers. In fact, the intermediate regime is itself a crossover regime between the high and the low temperature regime.

- The high temperature regime, $T >> T_K$. The coupling J is weak. Electrons rarely scatter of the magnetic moments. The resistivity is dominated by electron–phonon scattering. The susceptibility obeys a Curie–Weiss law $\chi = \frac{A}{T+\Theta}$ with antiferromagnetic (positive) Curie–Weiss temperature Θ.
- The onset of screening at intermediate temperatures, $T \sim T_K$. The coupling J grows logarithmically, leading to stronger scattering. The screening cloud starts to form but is too incomplete to mask the growing coupling. Since the phonons are frozen out, the resistivity grows logarithmically. The susceptibility also behaves logarithmically in this regime.
- The low temperature regime, $T << T_K$. The coupling J is very strong, leading to a quasi–bound state of the impurity with the surrounding electrons. The impurities are screened, so that the electrons are in a Fermi liquid state. Consequently, both resistivity and susceptibility approach their finite $T = 0$ values with quadratic T–dependence.

Nozières [25] presented a phenomenological Fermi liquid picture for the low temperature state. Several groups [17–22] applied the Bethe ansatz technique to solve exactly for the energy spectrum of the Kondo model. This provided the first exact analytical results for thermodynamic properties. Conformal Field Theory was employed by Affleck and Ludwig [26,27] and Bosonization techniques by Haldane [28] and Emery and Kivelson [29] to obtain exact statements for self energies in the strong coupling, low temperature regime. However, even today there is no technique available, which allows for exact evaluation of dynamic properties at all temperatures. The knowledge of the dynamics of the system is crucial for the determination of nonequilibrium properties. In the next chapter I will describe an approximative technique which can provide qualitative and sometimes quantitative correct results in all regimes.

3.3 Two Channel Kondo Systems and the Overscreened Kondo Effect

A basic assumption of the Kondo model Eq. 2.2 is that due to the locality of the interaction only the s–wave component of the electrons interacts with the magnetic moment. In principle, higher partial waves (p–wave, d–wave) could also couple to the local moment. If angular momentum is a good quantum number, it is conserved. This means that different partial waves act like different species of electrons coupled to the local moments. This picture leads to the multichannel Kondo model introduced by Nozières and Blandin [13]. In this model M species or 'channels' of mutually noninteracting electrons couple to a dilute concentration of local moments. In general, the moments can have any spin, but I am mostly

interested in spin–1/2 impurities. The hamiltonian might have the following form:

$$H = \sum_{p,\sigma\tau} (\epsilon_p - \mu) c^\dagger_{p\sigma\tau} c_{p\sigma\tau} - J\vec{S} \sum_{\tau} \sum_{p,p',\alpha,\beta} c^\dagger_{p\alpha\tau} \vec{\sigma}_{\alpha\beta} c_{p\beta\tau} \tag{3.1}$$

The new index $\tau = 1 \ldots M$ labels the M channels.

Possible realizations of the model Eq. 3.1 include the quadrupolar Kondo model introduced by Cox [30], possibly relevant for certain heavy fermion compounds [31, 32], and the Kondo model of Two Level Systems (TLS) first studied by Vladar and Zawadowski [33–37]. In the latter model there is a confusing switch of the active and passive degree of freedom. In the straightforward generalization of the Kondo model described above, the impurities and the electrons interact via a spin interaction. Thus, the spin is the active degree of freedom, whereas the channel degree of freedom (the partial wave index) is unaltered by the interaction.

In the Kondo model of Two Level Systems, these roles are reversed. The TLS is usually thought of as an atom with two energetically degenerate positions embedded in a bulk matrix (in this case a metal). Since the TLS is explicitly nonlocal, it will certainly interact with different partial waves. On the other hand, there is nothing magnetic in the system, i.e. one does not have a local electronic level (like in the Anderson model) hopping with the atom. This means spin is a good quantum number and is unchanged by the interaction with the TLS. However, the electrons can change their partial waves index by interaction with the TLS. This means there are processes in which the electron assists the

TLS to change its state (the atom hops from one position to the other) but pays the price of having to change its partial wave index. Therefore, the partial wave index is the active degree of freedom altered by the interaction whereas the spin remains unchanged and serves as the channel index in this case. Since the electrons carry spin 1/2, the above reasoning leads to a $M = 2$ channel Kondo model, with degeneracy $N = 2$ due to the two states of the TLS.

The above discussion, although specific for illustrative purposes, is only an example of how to create a channel Kondo model with a TLS. However, the specific realization of the TLS and its interaction with different partial wave or superpositions of partial waves (e.g. of different parity) is unimportant (and not known for most systems, except for certain glasses). As long as there is an interaction which allows changes in the active degree of freedom (e.g. partial waves, parity) and no magnetic interaction, the spin of the electrons provides the two channels to the Kondo effect of the active degree of freedom with the TLS. This implies that two channel Kondo systems should be rather common. The question then arises why systems with such peculiar behavior (described below) have not been observed until recently.

A possible answer to that question is that the assumption of at least near degeneracy of the two states of the TLS is not very often fulfilled. If the asymmetry Δ of the two states is too large, there will be no Kondo effect at all at temperatures $T < \Delta$. Essentially, the system will be weakly interacting with some potential scattering. At higher temperatures other effects like phonons will obscure any symptoms of two channel Kondo behavior. Only if there is a

large enough range between the temperature below which phonons are frozen out and the asymmetry Δ can one hope to observe the unusual two channel Kondo physics.

Although the hamiltonian Eq. 3.1 looks deceptively similar to the original, single channel hamiltonian Eq. 2.2, the low temperature physics for the case of $M = 2$ channels and degeneracy $N = 2$ is radically different from the standard, single channel Kondo model. This can be understood by noting that the impurity is now *overscreened.* In the language of the magnetic Kondo effect one can say that at low T the impurity would like to from a singlet state with a single electron. However, if there are two species of electrons (e.g. red and blue electrons), each specie interacts with the same strength with the impurity, so that if a red electron binds to the impurity, a blue electron will do so as well. Due to the antiferromagnetic coupling the spins of the red and blue electrons will be of opposite sign as that of the impurity. Because the size of the spin of the impurity and each electron is the same, the combined object of impurity and the red and blue electrons cannot form a spin singlet, but will again be a spin $1/2$ object with spin opposite to the original impurity spin.

This composite object will again try to bind another pair of red and blue electrons with opposite spin. Again, the combined object, now consisting of the impurity and two pairs of red and blue electrons with opposite spin, is a spin $1/2$ object with the same spin as the original impurity. This scenario can be continued ad infinitum. The difference to the original Kondo effect is obvious. Whereas in the single channel model the impurity spin was effectively screened at distances

larger than $\xi_K \sim v_F/T_K$ (v_F is the Fermi velocity), in the two channel case, there is no such screening. All electrons feel the full strength of the coupling J. This coupling does not actually diverge as in the standard Kondo model, but it is large enough to radically change the ground state of the system at low temperatures.

No longer can the low T physics be described by a Fermi liquid of weakly interacting electrons. All states are many–body states of strongly interacting particles. Due to the lack of screening the intermediate regime crosses over to a new Non–Fermi Liquid (NFL) regime at temperatures $T << T_K$. Nonperturbative methods are again necessary to obtain the thermodynamic and transport properties. All the techniques mentioned previously have been applied. The main results are as follows:

- A logarithmic divergence of the susceptibility at low T, $\chi \sim -\log(T/T_K)$ rather than the finite Pauli susceptibility of the single channel model.
- The resistivity shows nonanalytic power law behavior, $\rho = \rho_o(1 - T^{1/2})$, in contrast to the quadratic Fermi liquid behavior.
- The $T = 0$ entropy is *nonzero*, $S = 1/2 \ln 2$ per impurity. This implies a residual degree of freedom 'half' of a spin 1/2 impurity. The situation is somewhat similar to a frustrated spin system.

I mentioned above that the Kondo effect is among the most fascinating examples of many–body physics. The two channel Kondo systems is in some respects even more fascinating, being a non–Fermi liquid at low temperatures. On the other hand, it is somewhat simpler to treat once one has dealt with the strong

interactions precisely because there is no 'new' Fermi liquid behavior emerging as one lowers T from the intermediate regime. It is this feature which renders the approximation I will describe in the next chapter essentially exact, even and in particular at the lowest temperatures.

It is rather amusing that the two channel Kondo model, which is supposedly more complicated, can be very well described at all relevant temperatures, even out of equilibrium, by a single technique, the Non–Crossing Approximation (NCA). In contrast, for the single channel Kondo model, in the focus of attention for more than 30 years, such a technique has yet to be found.

CHAPTER 4
SLAVE BOSON TECHNIQUE AND THE NONCROSSING APPROXIMATION (NCA)

Before introducing the slave boson representation and discussing the Non Crossing Approximation (NCA), I have to say more about the specific systems I am going to consider. The previous chapters dealt with dilute concentrations of Kondo or Anderson impurities in a metallic bulk. If I apply a small bias V to the sample, the electrons about the impurities are essentially in local equilibrium. In this case I can apply linear response theory and obtain results for e.g. the resistivity.

I will be mainly interested in nonequilibrium situations, where it is no longer possible to consider the electrons about the impurities in local equilibrium. Such a situation can be achieved in a tunnel junction or a point contact. For a tunnel junction this quite obvious: If the impurities are located in the insulating layer between two clean metallic leads, an applied bias will drop almost entirely over the range of the insulating layer, leading to a nonequilibrium distribution of electrons about the impurities. For a small point contact the situation is similar. A point contact consists of two metal leads joined by a narrow constriction. Again, any applied bias will drop over a range of the size of the point contact. If this size is small and the impurities sit exclusively in the constriction, I again deal with a nonequilibrium distribution of electrons about the impurities.

For concreteness, I will discuss the technique in terms of a tunnel junction.

The model under consideration is a multichannel Kondo model as described by Eq. 3.1, where the impurity sits in the middle of the insulating layer between the two metallic leads. For the single channel case such a model was introduced by Appelbaum [38] and Anderson [39]. Because I assume the impurity in the exact middle, the bias V will only appear as shifts of the chemical potentials (i.e. the Fermi level) of the leads. This case is generic, although more general situations can be considered and are discussed in [40].

4.1 Slave Boson Hamiltonian

In chapter 2 and 3 I have described the equivalence of the Kondo model and the Anderson model in the Kondo limit. This equivalence can also be used for the multichannel models. Instead of trying to solve the multichannel Kondo model, I will use the multichannel Anderson model as the starting point. The Anderson hamiltonian of a tunnel junction with applied bias V reads

$$\begin{aligned} H = & \sum_{p,\sigma,\tau,\alpha} (\epsilon_p - \mu_\alpha) c^{\alpha\,\dagger}_{p\sigma\tau} c^{\alpha}_{p\sigma\tau} \\ & + \epsilon_d \sum_{\sigma\tau} d^\dagger_{\sigma\tau} d_{\sigma\tau} + U \sum_{\sigma\sigma'\tau} d^\dagger_{\sigma\tau} d_{\sigma\tau} d^\dagger_{\sigma'\tau} d_{\sigma'\tau} \\ & + \sum_{p,\sigma,\tau,\alpha} W_\alpha (d^\dagger_{\sigma\tau} c^\alpha_{p\sigma\tau} + h.c.), \end{aligned} \tag{4.1}$$

where the first term describes the conduction electron bands labeled by their (pseudo–) spin $\sigma = 1 \dots N$ and their channel index, $\tau = 1 \dots M$. In the presence of an external bias V, the conduction electrons to the left and right of the junction also have different chemical potentials μ_α, $\alpha = L, R$. The second and third

terms describe the impurity level ϵ_d and the interaction of electrons on the level, respectively. The fourth term describes the hybridization of the impurity level with the conduction electrons on either side of the junction.

This is a model of an impurity level far below the Fermi surface ($\epsilon_d << 0$) hybridizing with the M channels of conduction electrons. U has to be the largest energy (in magnitude) for the mapping of the Anderson to Kondo model (the Schrieffer–Wolff transformation [6]) to be valid. For convenience, I take the limit $U \to \infty$. This makes double occupancy of the impurity level impossible. Barnes [41] has introduced the 'slave boson decomposition' of the electron operators on the level, $d^\dagger_{\sigma\tau}, d_{\sigma\tau}$, by writing

$$d^\dagger_{\sigma\tau} = f^\dagger_\sigma b_\tau, \quad d_{\sigma\tau} = b^\dagger_\tau f_\sigma \tag{4.2}$$

where f and b are canonical fermion and boson operators, respectively. The constraint of no double occupancy in terms of the electron operators $d^\dagger, d$ is an inequality, $\sum_{\sigma\tau} d^\dagger_{\sigma\tau} d_{\sigma\tau} \leq 1$. This means that either the level is empty or it is occupied by a single electron. With the slave boson decomposition, the constraint of no double occupancy can now be written as an exact constraint on the new operators f and b:

$$Q = \sum_\sigma f^\dagger_\sigma f_\sigma + \sum \tau b^\dagger_\tau b_\tau = 1 \tag{4.3}$$

In terms of the slave boson operators, the hamiltonian 4.1 reads

$$H = \sum_{p,\sigma,\tau,\alpha} (\epsilon_p - \mu_\alpha) c^{\alpha\,\dagger}_{p\sigma\tau} c^\alpha_{p\sigma\tau} + \epsilon_d \sum_\tau f^\dagger_\tau f_\tau$$

$$+\sum_{p,\sigma,\tau,\alpha} W_\alpha(f^\dagger_\tau b_{\bar{\sigma}} c^\alpha_{p\sigma\tau} + h.c.). \tag{4.4}$$

This hamiltonian has to be supplemented by the constraint Q, which restricts its action to the physical Hibert space. The constraint can be enforced in the standard way by introducing a Lagrange–multiplier λ and adding a term $\lambda(Q-1)$. The technique of how to perform perturbation theory and obtain physical properties is described at length in the review of Bickers [12]. The general method involves computation in the unrestricted Hilbert space where Q can have any value. Then, one projects onto the physical Hilbert space with $Q = 1$ by letting $\lambda \to \infty$ which eliminates any contributions from states with $Q > 1$. The states with $Q = 0$ can be eliminated, too. The result are expressions for physical properties in terms of the projected slave particle Green functions. Below I will show these expressions for the quantities of interest.

4.2 The Non Crossing Approximation (NCA)

4.2.1 Validity of the NCA

The strength of the slave boson formalism is that it treats the largest energy, the on–site repulsion U exactly (for $U = \infty$), rather than perturbatively. The NCA is a self–consistent perturbation approximation for the self energies of the slave particles, $\Sigma(\omega)$ (fermion) and $\Pi(\omega)$ (boson) in the coupling of band electrons to the impurity level W. The second order expressions are made self–consistent by inserting the dressed slave particle propagators in the Feynman diagrams instead of the bare propagators [9–12]. One can show that this amounts to

the summation of all self energy diagrams (in Matsubara frequency space) for which no propagators are crossing each other (thus the name: Non Crossing Approximation) [9]. If one considers the degeneracy N as a variable and performs an $1/N$–expansion, one can also show that the NCA accounts for all diagrams up to order $O(1/N)$. All other diagrams, including all vertex corrections, are at least of order $O(1/N^2)$ and may thus be neglected in the limit of large N. I am mostly concerned with degeneracies $N = 2$, i.e. Two Level systems. It is not obvious that an approximation which is valid for large N gives at least qualitatively correct results for $N = 2$.

The NCA has been very successful in describing the single channel Kondo model, except for the appearance of spurious nonanalytic behavior at temperatures far below the Kondo temperature T_K. This does not really limit the application to physical systems, since there is a wide temperature range well above the energy scale of these NCA– artifacts and still well below the T_K. The spurious low-T properties are due to the fact that the NCA neglects vertex corrections responsible for restoring the low T Fermi liquid behavior of the one channel model [42]. However, it has recently been shown [43] that for the two channel problem, where the complications of the appearance of a Fermi liquid fixed point are not present, the NCA does give the exact low-frequency power law behavior of the impurity spectral function $A_d(\omega)$ and the suceptibilities at zero T. Therefore, I expect to achieve a correct description for quantities involving A_d (like the conductance) and the susceptibilities even at the lowest temperatures which can be reached within reasonable numerical effort (about $1/1000\ T_K$).

4.2.2 NCA for the Equilibrium Case

The equations for the self energies of the retarded Green functions $G^r(\omega) = (\omega - \epsilon_d - \Sigma^r(\omega))^{-1}$ (fermion) and $D^r(\omega) = (\omega - \Pi^r(\omega))^{-1}$ (boson) read [12, 44]

$$\begin{aligned} \Sigma^r(\omega) &= \frac{M}{\pi} \int d\epsilon \Gamma(\omega - \epsilon)(1 - F(\omega - \epsilon)) D^r(\epsilon) \\ \Pi^r(\omega) &= \frac{N}{\pi} \int d\epsilon \Gamma(\epsilon - \omega) F(\epsilon - \omega) G^r(\epsilon) \ , \end{aligned} \tag{4.5}$$

where $\Gamma(\omega) = \pi |W|^2 N(\omega) = \Gamma N(\omega)$ ($N(\omega)$ is the density of states of the band electrons) and $F(\omega) = 1/(1 + e^{\beta\omega})$ is the Fermi function. The self energies are complex functions of ω. However, due to analyticity at finite temperatures, the real and imaginary parts are not independent. They can be obtained from each other by means of a Kramers–Kronig relation, e.g.

$$Re\Sigma^r(\omega) = \frac{1}{\pi} P \int d\epsilon \frac{\mathrm{Im}\Sigma^r(\epsilon)}{\epsilon - \omega}, \tag{4.6}$$

where P in front of the integral indicates Cauchy's principal value. Taking the imaginary part of Eqs. 4.5 and defining the spectral functions for the slave particles

$$A(\omega) = -\mathrm{Im} G^r(\omega)/\pi = -\mathrm{Im}\Sigma^r \, |G^r|^2/\pi$$

$$B(\omega) = -\mathrm{Im} D^r(\omega)/\pi = -\mathrm{Im}\Sigma^r \, |D^r|^2/\pi \, ,$$

I arrive at

$$\frac{A(\omega)}{|G^r(\omega)|^2} = \frac{M}{\pi} \int d\epsilon \Gamma(\omega - \epsilon)(1 - F(\omega - \epsilon)) B(\epsilon)$$

$$\frac{B(\omega)}{|G^r(\omega)|^2} = \frac{N}{\pi} \int d\epsilon \Gamma(\epsilon - \omega) F(\epsilon - \omega) A(\epsilon) \ . \tag{4.7}$$

Together with Eq. 4.6 (and the bosonic complement) Eqs. 4.7 form a complete set of equations to determine the Green and spectral functions of the slave particles.

However, this is not enough to compute the impurity spectral function $A_d(\omega)$ at low temperatures (the zero temperature limit). This becomes obvious by looking at the corresponding expression [11]

$$A_d(\omega) = \frac{1}{Z} \int d\epsilon \, e^{-\beta\epsilon} \left[A(\epsilon + \omega) B(\epsilon) + A(\epsilon) B(\epsilon - \omega) \right], \tag{4.8}$$

where

$$Z = \int d\epsilon \, e^{-\beta\epsilon} [N A(\epsilon) + M B(\epsilon)] \tag{4.9}$$

is the partition function of the impurity in the physical Hilbert space. The Boltzmann–factor does not allow for a numerical evaluation of the integrand at negative ϵ if $\beta = 1/k_B T$ is large. It is therefore necessary to include the Boltzmann–factor in the spectral functions and find solutions for the functions

$$a(\omega) = e^{-\beta\omega} A(\omega) \ , \quad b(\omega) = e^{-\beta\omega} B(\omega) \ . \tag{4.10}$$

The corresponding equations are easily found from Eqs. 4.7. I can absorb the

Boltzmann–factor by making use of the relation $F(-\omega) = 1 - F(\omega) = e^{\beta\omega}F(\omega)$.

$$\frac{a(\omega)}{|G^r(\omega)|^2} = \frac{M}{\pi}\int d\epsilon\Gamma(\omega-\epsilon)(F(\omega-\epsilon))b(\epsilon)$$
$$\frac{b(\omega)}{|G^r(\omega)|^2} = \frac{N}{\pi}\int d\epsilon\Gamma(\epsilon-\omega)(1-F(\epsilon-\omega)a(\epsilon)\ . \tag{4.11}$$

With the functions a and b the equations for the impurity spectral function and the partition function are

$$A_d(\omega) = \frac{1}{Z}\int d\epsilon\,[\,A(\epsilon+\omega)b(\epsilon) + a(\epsilon)B(\epsilon-\omega)] \tag{4.12}$$

$$Z = \int d\epsilon\,[Na(\epsilon) + Mb(\epsilon)]\ . \tag{4.13}$$

It is instructive to realize that the functions a and b are proportional to the Fourier transform of the lesser Green functions, that is

$$a(\omega) = \frac{i}{2\pi}G^<(\omega),\quad G^<(t-t') = -i\langle\, f^\dagger(t')f(t)\,\rangle \tag{4.14}$$
$$b(\omega) = \frac{i}{2\pi}D^<(\omega),\quad D^<(t-t') = i\langle\, b^\dagger(t')b(t)\rangle \tag{4.15}$$

and are proportional to the distribution functions of the slave particles. From now on I call $a(\omega)$ and $b(\omega)$ the 'lesser' functions. Eq. 4.13 tells me that Z is obtained by integrating the lesser functions with the corresponding degeneracies

N and M multiplied. This implies that Z is the averaged constraint, that is

$$Z = \langle \sum_{\tau} f_{\tau}^{\dagger} f_{\tau} + \sum_{\bar{\sigma}} b_{\bar{\sigma}}^{\dagger} b_{\bar{\sigma}} \rangle = 1 \,, \tag{4.16}$$

where the angular brackets denote the expectation value in the general Hilbert space with the projection on the physical Hilbert space imposed after the computation of this expectation value.

The Eqs. 4.6, 4.7 and 4.11 form a set of equations which allow for the construction of the impurity spectral function A_d (from which most transport properties follow). The equations are solved by iteration with gaussians as initial 'guesses' for the spectral and lesser functions at high temperatures. Once solutions for high T are found (that is, the solutions are so stable under further iteration that no function value at any frequency changes more than 0.1%), the next job at lower T will use these solutions as input functions. Temperatures down to $1/1000\ T_K$ can be reached upon repeating this procedure. After finding such low–T solutions, it is favorable (since faster) to use these solutions as input.

A general problem of iterative solutions of integral equations is convergence and/or convergence to the 'right' (physical) solutions. If I end up with solutions that do not fulfill the constraint $Z = 1$, all effort was in vain. There is an elegant way to enforce the constraint at every iteration step which I will describe in Appendix A. Sum rules constitute other checks the solutions have to fulfill. The slave particle spectral functions should be normalized to unity, whereas the impurity spectral function must fulfill $\int d\epsilon A_d(\epsilon) = 1 - (1 - 1/N)n_f$, with n_f the fermion occupation number. Also, $n_d = n_f$ must hold (n_d is the real electron

occupation number per spin (parity)). All these conditions are fulfilled to within 0.5% in the worst cases (low T, etc.) but typically they do even better (0.1%). I conclude that the solutions fulfill all physical constraints very well.

A dramatic simplification of the above procedure can be achieved that is special to the equilibrium case. I note that the relation between the spectral and the lesser functions is known and given by Eq. 4.10. This motivates me to define new functions $\tilde{A}(\omega)$ and $\tilde{B}(\omega)$ by

$$\tilde{A}(\omega) = \frac{A(\omega)}{F(-\omega)}\ , \quad \tilde{B}(\omega) = \frac{B(\omega)}{F(-\omega)}\ . \tag{4.17}$$

If I could find these functions by some procedure, the lesser and the spectral functions would follow by multiplication of factors that are well behaved in the zero temperature limit. For the spectral functions the corresponding factor is by definition $F(-\omega)$, whereas for the lesser function I find

$$a(\omega) = e^{-\beta\omega}A(\omega) = e^{-\beta\omega}F(-\omega)\tilde{A}(\omega) = F(\omega)\tilde{A}(\omega)\ . \tag{4.18}$$

Indeed, it poses no problem to find equations for $\tilde{A}(\omega)$ and $\tilde{B}(\omega)$ in very much the same way as I found the equations for the lesser functions from Eqs. 4.7 for the spectral functions. The results are

$$\begin{aligned}\frac{\tilde{A}(\omega)}{|G^r(\omega)|^2} &= \frac{M}{\pi}\int d\epsilon\Gamma(\omega-\epsilon)\frac{(1-F(\omega-\epsilon))F(-\epsilon)}{F(-\omega)}\tilde{B}(\epsilon)\\ \frac{\tilde{B}(\omega)}{|G^r(\omega)|^2} &= \frac{N}{\pi}\int d\epsilon\Gamma(\epsilon-\omega)\frac{F(\epsilon-\omega)F(-\epsilon)}{F(-\omega)}\tilde{A}(\epsilon).\end{aligned} \tag{4.19}$$

One can convince oneself that the products of Fermi functions in these equations are completely well behaved in the zero temperature limit. Thus, by solving the **two** Eqs. 4.19 instead of the **four** Eqs. 4.7 and 4.11 I can save one third of the integrations I have to perform per iteration (recall the two integrations in Eq. 4.6 and bosonic complement). Using this procedure a typical job on a decent workstation takes between two and five minutes (depending on T).

4.2.3 NCA for Static Nonequilibrium

If I apply a finite bias V by setting $\mu_L = +V/2$ and $\mu_R = -V/2$, the system is no longer in equilibrium. The NCA equations have to be derived by means of standard nonequilibrium Green function techniques [45]. Most important, one can **not** expect the simple relation Eq. 4.10 (or some naive modification) between the lesser and the spectral functions to hold. Therefore, the trick with introducing the functions $\tilde{A}$ and $\tilde{B}$ can not be performed. One has to solve the equivalent of Eqs. 4.7 and 4.11 for the nonequilibrium case without any further simplification. This was done first by Meir and Wingreen [46]. However, their derivation uses a Lorentzian density of states, which, though formally favorable, has disadvantages in the numerical evaluation. I follow an independent derivation, which allows for an arbitrary density of states [40, 47].

The NCA equations for static nonequilibrium read (recall $\Gamma(\omega) = \Gamma N(\omega)$)

$$\begin{aligned}\frac{A(\omega)}{|G^r(\omega)|^2} &= \frac{M}{\pi}\int d\epsilon B(\epsilon)\sum_\alpha[\Gamma_\alpha N(\omega-\epsilon+\mu_\alpha)(1-F(\omega-\epsilon+\mu_\alpha))] \\ \frac{B(\omega)}{|G^r(\omega)|^2} &= \frac{N}{\pi}\int d\epsilon A(\epsilon)\sum_\alpha[\Gamma_\alpha N(\epsilon-\omega-\mu_\alpha)F(\epsilon-\omega-\mu_\alpha)] \end{aligned} \quad (4.20)$$

$$\frac{a(\omega)}{|G^r(\omega)|^2} = \frac{M}{\pi}\int d\epsilon\, b(\epsilon)\sum_\alpha [\Gamma_\alpha N(\omega-\epsilon+\mu_\alpha)(F(\omega-\epsilon+\mu_\alpha))]$$
$$\frac{b(\omega)}{|G^r(\omega)|^2} = \frac{N}{\pi}\int d\epsilon\, a(\epsilon)\sum_\alpha [\Gamma_\alpha N(\epsilon-\omega-\mu_\alpha)(1-F(\epsilon-\omega-\mu_\alpha)] \quad (4.21)$$

If the density of states $N(\omega)$ were a constant, the only difference between the equilibrium and the nonequilibrium NCA equations would be the replacement of the Fermi function as a distribution function by an effective distribution function F_{eff} given by ($\Gamma_{tot} = \Gamma_L + \Gamma_R$)

$$F_{\text{eff}}(\epsilon) = \frac{\Gamma_L}{\Gamma_{tot}}F(\epsilon-\mu_L) + \frac{\Gamma_R}{\Gamma_{tot}}F(\epsilon-\mu_R) \quad (4.22)$$

Since my density of states is a gaussian with a width larger than all other energy scales (like $|\epsilon_d|$, Γ_{tot}, T_K) this is in fact the only significant modification of the NCA equations itself. Numerically, the most crucial modification concerns the integration mesh. The proper choice of integration meshes is central to the success of the iteration and is discussed extensively in Appendix B.

The NCA can also be generalized to the case where both the potentials in the leads and on the 'impurity' level are explicitly time–dependent, rather than static. For the case of harmonic oscillations of frequency Ω, I have computed the DC–current and DC–conductance in the nonadiabatic case, $\Omega >> T_K$ [48]. Many new features like electron pump effects and side peaks in the nonlinear conductance are predicted. However, inclusion of this material does not fit into the frame of this thesis.

4.3 Current Formulae, Conductance and Susceptibilities

4.3.1 Current Formulae and Conductance

Due to the finite bias V a current will flow from left to right through the impurity. This current can be computed from A_d alone, if, and only if, the couplings Γ_α of the impurity to the leads are the same, and if I assume a wide band that is flat for energies of order V about the Fermi level.

$$I(V) = \frac{Ne\Gamma_{tot}N(0)}{\hbar} \int d\omega A_d(\omega)[F(\omega - \mu_L) - F(\omega - \mu_R)]. \tag{4.23}$$

If the couplings are not equal, another term shows up [49,50], involving the lesser Green function $G_d^<$ of the impurity electrons. $G_d^<$ can be computed via

$$G_d^<(\omega) = \frac{1}{Z} \int d\epsilon\, a(\epsilon)B(\epsilon - \omega) \ . \tag{4.24}$$

The NCA is a current conserving approximation [46]. Therefore, the currents computed for the left and the right leads should be the same when formally evaluated. For general couplings and bands, the left and right currents are given by

$$I_L(V) = \frac{-Ne}{\hbar} \int d\omega \Gamma_L N(\omega - \mu_L) \left[G_d^<(\omega) - A_d(\omega)F(\omega - \mu_L)\right] \tag{4.25}$$

$$I_R(V) = \frac{Ne}{\hbar} \int d\omega \Gamma_R N(\omega - \mu_R) \left[G_d^<(\omega) - A_d(\omega)F(\omega - \mu_R)\right] \tag{4.26}$$

Numerically, they agree better than 0.5%, which sets a limit to the uncertainty for the current $I(V) = (I_L + I_R)/2$.

In order to obtain the (differential) conductance $G(V) = dI(V)/dV$, I perform

a numerical derivative, using $(I(V_1) - I(V_2))/(V_1 - V_2)$, and take it as the value of G at the midpoint $(V_1 + V_2)/2$. This method does not smooth fluctuations induced by the numerics. If the currents are off by 0.5%, and if the difference $(V_1 - V_2)$ is small, the corresponding G could fluctuate wildly (20% and more). Such fluctuations of the conductance are not observed (at most 2% deviations in G), showing that the currents have a much smaller uncertainty than indicated by the difference of I_L and I_R (aside from overall shifts which do not effect the conductance).

To compute the zero bias conductance (ZBC), I can use either the equations above in the limit of $V \to 0$, or I can use equations obtained from linear response techniques. The latter method is favorable, since I only have to find the impurity spectral function *in equilibrium.* I use

$$G(0,T) = \frac{Ne^2\Gamma_{tot}N(0)}{\hbar} \int d\epsilon \frac{\partial F(\epsilon)}{\partial \epsilon} A_d(\epsilon) \tag{4.27}$$

for the ZBC in a tunnel junction.

Within linear response, I can also compute the bulk resistivity ρ of a small density of impurities in a bulk metal. ρ is related to the impurity spectral function via [12]

$$1/\rho = const \int d\epsilon \frac{\partial F(\epsilon)}{\partial \epsilon} \tau(\epsilon)\,, \tag{4.28}$$

where $\tau^{-1}(\epsilon) = CA_d(\epsilon)$ (C is impurity concentration) is the inverse scattering time. The constant in front of the integral is material dependent. Observe that because of the "double inversion" in the above expression the bulk resistivity ρ

decreases with temperature above T_K. In combination with the rise of ρ at higher temperatures due to phonon scattering, this leads to a resistivity minimum at a finite temperature.

Most of the calculations are done with symmetric couplings, $\Gamma_L = \Gamma_R$. However, especially for a tunnel junction this is probably not the realistic case. If the impurity is at some position x within the insulating layer of thickness d, the Γ_L will be larger (smaller) than Γ_R, if x is close to zero (d). Also, the bare energy level ϵ_d of the impurity will be shifted to higher (lower) values, if x is smaller (larger) than $d/2$. In order to keep the total coupling $\Gamma_{tot} = \Gamma_L + \Gamma_R$ constant (and for simplicity), I assume a linear dependence of the Γ_α's on x of the form $\Gamma_L = \Gamma_{tot}(1 - x/d)$, $\Gamma_R = \Gamma_{tot} x/d$. I also modify ϵ_d according to $\epsilon_d(V) = \epsilon_d + (V/2)(1 - 2x/d)$. The latter modification turns out to be insignificant as long as $V << |\epsilon_d|$.

In Ref. [40] I show that asymmetric couplings actually lead to a conductance peak (zero bias anomaly) that is asymmetric about zero bias. Such asymmetries have indeed been observed in experiments on tunnel junctions. Since this is only a side issue, I refrain from just reproducing the data and refer the reader to Ref. [40].

4.3.2 Tunnel Junctions vs. Point Contacts

The above formulae for the currents and conductances are valid in a tunnel junction geometry where the current must flow through the impurity. In a point contact two leads are joined by a small constriction. A current I_o will flow through the constriction without the impurity being present. In fact, the impurity will

impede the current, due to additional scattering in the vicinity of the constriction. The question arises whether the effect of the impurity in a point contact is the same in magnitude but with a different sign as in the tunnel junction. In Ref. [40] I consider a simple (one–dimensional) model. I find that indeed the switch of signs is the only effect on the current due to the impurity, provided the transmittance t of the constriction is close to unity, $t \sim 1$. Thus, in clean samples the results for the current calculated for the tunnel junction apply for point contact, too, if one subtracts the impurity contribution from the background current I_o. If I_o is ohmic, the conductance $G(V)$ is shifted by a the constant dI_o/dV. Aside of this shift, the conductance signals of a tunnel junction and a clean point contact will be the same except for the sign.

4.3.3 Susceptibilities

The (dynamic) susceptibility is calculated using the standard formulae [11,12] from the lesser and the spectral function of the fermions alone. The formula for the imaginary part reads

$$\mathrm{Im}\chi(\omega) = \frac{1}{Z}\int d\epsilon \, [\, A(\epsilon+\omega)a(\epsilon) - a(\epsilon)A(\epsilon-\omega)] \ . \tag{4.29}$$

The real part can be obtained from the imaginary part by means of a Kramers–Kronig relation.

$$\mathrm{Re}\chi(\omega) = \frac{1}{\pi}P\int d\epsilon \frac{\mathrm{Im}\chi(\epsilon)}{\epsilon-\omega} \tag{4.30}$$

The static susceptibility $\chi_o = \mathrm{Re}\chi(\omega = 0)$ follows from this expression.

In the two channel Anderson model this susceptibility is *not* the magnetic susceptibility, since the spin of the electrons does not couple to the 'impurity' (TLS). The magnetic susceptibility is then given by the formulae above with the fermionic lesser and spectral functions replaced by their bosonic counterparts.

CHAPTER 5
SCALING PROPERTIES OF SELF ENERGY AND CONDUCTANCE

In this chapter I present the results from the numerical evaluation of conductance and bulk resistivity for the case of symmetric couplings to the leads, using the formulae discussed in the previous sections.

The results for the two channel case and the nonlinear conductances have been computed for a point contact. For the one channel case I show the zero bias conductance (ZBC) for a tunnel junction in Fig. 5.2 in order to compare directly to the bulk resistivity ρ of a metal with Kondo–impurities in Fig. 5.3. The data for the two channel case have been mostly presented before in Ref. [47]. The one channel data are presented to contrast the two channel results and to show the failure of the NCA in reproducing the correct scaling exponent for $N = 2$.

5.1 Linear Response Conductances and Resistivity

In Fig. 5.1 I show the zero bias conductance $G(0,T)$, for the two channel case ($N = M = 2$). As expected [26, 27], the ZBC shows $T^{1/2}$ dependence at low T with deviations starting at about $1/4\ T_K$. T_K is chosen to be the width at half maximum of the zero bias impurity spectral function, A_d, at the lowest calculated T (see inset). The slope of the $T^{1/2}$ behavior defines the constant B_Σ:

$$G(0,T) - G(0,0) = B_\Sigma T^{1/2}. \tag{5.1}$$

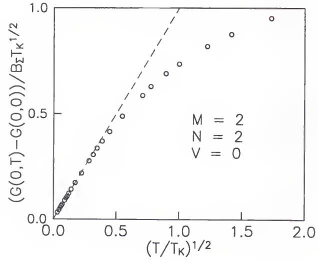

Figure 5.1: Temperature dependence of the zero bias conductance for the $M = 2$ channel case in a point contact. The zero bias conductance has $T^{1/2}$- dependence for $T < T_K/4$. This can be used to roughly extract T_K from the experimental data. B_Σ is a material dependent constant which has been divided out. Therefore, the slope of the low T fit (dashed line) is equal unity.

For the one channel case ($M = 1, N = 2$) one would naively expect T^2–behavior from the exact solution of the corresponding Kondo model (Fermi liquid behavior at low T). However, the NCA as a large N expansion is **not** able to obtain this power law for $N = 2$. Instead, the ZBC shows dominant linear T–dependence at low temperatures. As discussed in the next section the nonlinear conductance also has portions with the corresponding power law (linear for $N = 2$) as long as T and V are well below T_K.

For $N = 4$ and $N = 6$ the ZBC has humps at temperatures below T_K (Fig.

5.2, for a tunnel junction) because the Kondo resonance is shifted away from the Fermi level for $N > 2$. Similar humps can be seen in the magnetic susceptibilities of these systems [12].

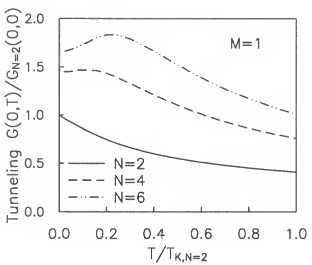

Figure 5.2: Zero bias conductance for a tunnel junction vs. temperature for the $M = 1$ channel model. The conductance for a clean point contact would be obtained by subtraction of this curve from a (constant) background conductance. The graph for $N = 2$ shows an almost linear T–dependence at low T whereas the curves for spin degeneracy $N = 4$ and 6 show nonmonotonic behavior (humps) The humps are due to the fact that the Kondo peak of the spectral function A_d is shifted away from the Fermi energy ϵ_F by about T_K. For $T > T_K$ all the curves fall like $\log(T/T_K)$ for approximately one decade.

For a bulk Kondo system it is impossible to measure the ZBC of single impurities. Instead, one can measure the resistivity ρ of the bulk metal. In Fig. 5.3 I show the low T parts of the resistivity for one channel impurities with $N = 2, 4, 6$. Only $N = 6$ shows a convex dependence on T. In fact, ρ behaves like $(1 - \alpha(T/T_K)^2)$, as expected for a Fermi liquid [12]. However, the NCA does not

reproduce Fermi liquid behavior for $N = 2$. Again, this is not surprising, since the NCA is an expansion valid for large values of N.

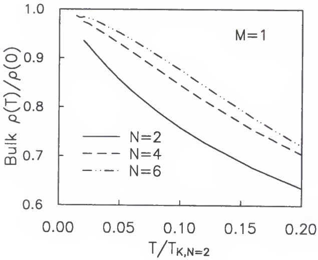

Figure 5.3: Bulk resistivity vs. temperature for the $M = 1$ channel model. Of the three curves only $N = 6$ has a clear convex shape and falls roughly like T^2 at low T. The $N = 2$ graph again shows almost linear T–dependence. Note that the humps in the conductance for $N = 4$ and 6 are not present in the bulk resistivity ρ.

5.2 Nonlinear Conductance

Recently, it has been shown [47] that the two channel model exhibits scaling of the nonlinear conductance $G(V, T)$ as a function of bias V and T of the form [14]

$$G(V, T) - G(0, T) = B_\Sigma T^\eta H((A\frac{eV}{k_B T})) \ , \tag{5.2}$$

but there are finite T corrections even for $T << T_K$. Here, H is a universal scaling function ($H(0) = 0$ and $H(x) \sim x^\eta$ for $x >> 1$) and B_Σ and A are nonuniversal constants. The exponent η is 1/2 for the two channel model. This scaling ansatz is motivated by the scaling of the self energy of the electrons in the variables frequency ω and temperature T as obtained by CFT in equilibrium [26,27]. Since such scaling is well known to be present in the $N = 2$ single channel case [12] I expect scaling of the conductance of the form Eq. 5.2, too, although the exponent η should equal 2 (Fermi liquid behavior) in this case.

In order to examine whether this ansatz is correct, the rescaled conductance is plotted as a function of $(eV/k_BT)^\eta$. The conductance graphs for different T should collapse to a single curve with a linear part for not too large arguments, e.g. $(eV/k_BT)^\eta < 4$ (since too large V or T would drive the system out of the scaling regime). Such a collapse indeed happens for low bias $V < T$. However, for larger bias the slope of the linear part shows T dependence (for more details see Ref. [47]). This is not contradictory to the scaling ansatz, but it does show that there are significant T–dependent corrections to scaling.

Fig. 5.4 a) and b) show the scaling plots for the cases $M = 2$ and $M = 1$, respectively ($N = 2$ in both cases). Whereas the two channel case shows the behavior described above with the expected exponent $\eta = 1/2$, the NCA does not give the correct exponent for the one channel model, that is, the standard Kondo model. In fact, the data show scaling, however, the exponent η is equal unity rather than 2. This seems to reflect the linear temperature dependence of the conductivity that the NCA produces in this case. This shortcoming is another

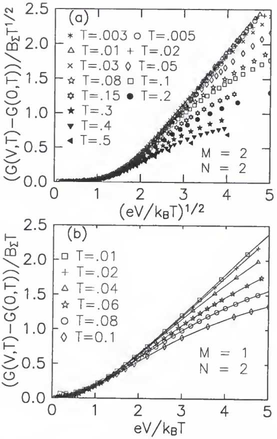

Figure 5.4: Scaling plots of the conductance for (a) the two channel case ($M = N = 2$), and (b) the one channel case ($M = 1, N = 2$) for point contacts. With $\Gamma_L = \Gamma_R$ and B_Σ determined from the zero bias conductance , there are no adjustable parameters. There are roughly two regimes in these plots. For $(eV/k_BT)^\eta < 1.5$ the curves collapse onto a single curve and the rescaled conductance is proportional to $(eV/k_BT)^2$. For larger $(eV/k_BT)^\eta$ the rescaled conductance is linear on these plots. There are substantial corrections to scaling even at T small compared to T_K. At even larger biases this linear behavior rounds off, indicating the breakdown of scaling. The temperatures are in units of T_K, which is different for the two cases.

consequence of the negligence of vertex–corrections within the NCA, or, in other words, a consequence of using an $1/N$–expansion at $N = 2$. On the other hand, the fact that scaling is present again shows that the qualitative behavior is well reproduced.

CHAPTER 6
SUSCEPTIBILITY IN AND OUT OF EQUILIBRIUM

6.1 Equilibrium Susceptibility for the Two Channel Model

Finally, I also show results for the static and dynamic susceptibilities with and without finite bias. All data shown are for the two channel model. The results for the usual Kondo model show different power laws, but the general behavior upon application of a finite bias very similar.

In equilibrium, in the zero temperature limit, the dynamic susceptibility defined in Eq. 4.29 is given by a step function of the form [43]

$$\mathrm{Im}\chi(\omega) = c_1 \mathrm{sign}(\omega)[1 - c_2\sqrt{\omega/T_K} + \dots \quad . \tag{6.1}$$

The NCA approaches this behavior as the temperature is reduced. However, as shown in Fig. 6.1 the step is always broadened by the finite temperature with the extrema located at values which grow roughly with $T^{1/2}$. The real part follows by the Kramers-Kronig relation and would diverge logarithmically, but the temperature cuts off this divergence as well. As a consequence, the static susceptibility χ_o diverges logarithmically as T approaches zero, a non–Fermi liquid behavior predicted before [19, 26, 27, 35, 43] and well reproduced by the NCA technique, as shown in Fig. 6.2 (circles).

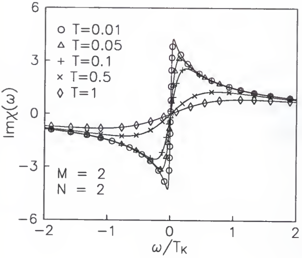

Figure 6.1: Dynamic susceptibility for the $M = 2$ channel case in equilibrium ($V = 0$). The graph shows how the dynamic susceptibility approaches a leading order step function as the temperature goes to zero, as expected for the two channel case (see Eq. 23). This is in contrast to the linear behavior of the $M = 1$ channel model. The value of the susceptibility is in arbitrary units.

6.2 Nonequilibrium Susceptibility for the Two Channel Model

Out of equilibrium, the finite bias serves as another low energy cutoff, but in a nontrivial manner. The extrema of the imaginary part of the susceptibility are located at smaller absolute values than at the corresponding temperature at zero bias. The logarithmic divergence of the real part is cut off at about V, so that the static susceptibility does not diverge logarithmically anymore as $T \to 0$. Instead, it approaches a (V–dependent) finite value with a quadratic T–dependence. However, this does not signal the return of Fermi liquid behavior for $T < V$, since there still is $\sqrt{V/T}$ behavior of the conductance for V well below

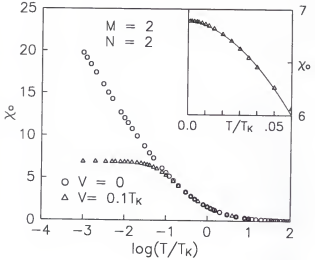

Figure 6.2: Static susceptibility χ_o vs. temperature for zero and finite bias V. In equilibrium, χ_o shows the characteristic, expected logarithmic divergence as T approaches zero (for the two channel model). Out of equilibrium, this divergence is cut off at a temperature somewhat below the bias V. The inset shows that χ_o falls with T^2 below this cutoff. For high temperatures $T >> T_K$, χ_o falls like $1/T$ (Curie–Weiss law). The value of the susceptibility is in arbitrary units.

T_K. Fig. 6.2 shows the T–dependence of χ_o for $V = 1/10T_K$ (triangles).

Similar behavior is observed in the V–dependence. Now T serves as a cutoff of the logarithmic divergence. For low V the static susceptibility saturates and falls quadratically with V. For $T < V < T_K$ the susceptibility then falls logarithmically. I show the V–dependence static susceptibility χ_o for various T in Fig. 6.3.

However, there is a difference in T and V in the regime $T_K < T, V < \Gamma_{tot}$. For large T the static susceptibility behaves like $1/T$, indicating Curie-Weiss behavior. However, for large bias χ_o falls less rapidly like $a/V + b\log(V)/V$.

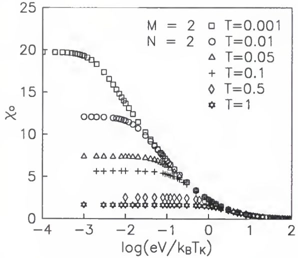

Figure 6.3: Static susceptibility χ_o vs. bias V for various temperatures T. χ_o has a very similar dependence on V and T as long as $V, T < T_K$ (in the scaling regime). χ_o drops first like V^2 and then like $\log(V)$. However, for large $V >> T_K$, χ_o falls less rapidly with V than with T, see the next figure. The value of the susceptibility is in arbitrary units.

This stresses again the different consequences of increasing T and V once one has left the scaling regime $T, V < T_K$.

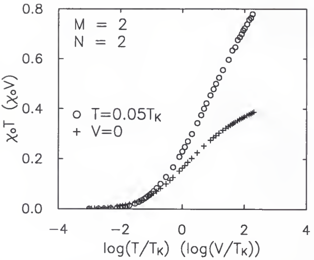

Figure 6.4: Product of the static susceptibility χ_o and temperature T (bias V) vs. T (V) on semi–logarithmic scale. The T–dependence shows saturation at high temperatures and therefore implies the Curie law, $\chi_o \propto 1/T$. However, the V–dependence is linear at large bias, implying that χ_o falls less rapidly with V than with T, $\chi_o \propto \log(V)/V$.

CHAPTER 7
CONCLUSIONS TO PART I

In conclusion, I described in detail the analytical foundations and numerical implementation of the NCA integral equations for the one and two channel Anderson model out of equilibrium. The algorithms enabled me to reach lower temperatures than previously obtained, allowing the study of new physics.

In linear response, I computed the conductance through a tunnel junction as well as the bulk resistivity. The two channel data for both properties show $T^{1/2}$–behavior in agreement with results obtained by other methods. For the one channel model and $N = 2$, I find dominant linear behavior at low temperatures. For $N = 6$, the bulk resistivity drops with T^2 (Fermi liquid behavior), however, the tunnel junction conductance *rises* with T^2, reaches a maximum below the Kondo temperature T_K and than falls of logarithmically at higher T. This "hump" is associated with the fact that the Kondo peak of the impurity spectral function is shifted away from the Fermi level for values of $N > 2$.

Out of equlibrium, the nonlinear conductance behaves again dominant linearly (for $T < V < T_K$) for the one channel case and $N = 2$. Therefore, I can plot the conductance as a function of eV/k_BT and achieve scaling for modest bias. Whether similar scaling of the conductance but with argument $(eV/k_BT)^2$ can exist for the case $N = 6$ is yet to be determined. The tunnel junction conductance falls with V^2 for bias $V < T_K$. This is not to reconcile with the hump in the

T–dependence of the zero bias conductance. If at all, scaling seems possible only for temperatures well below the temperature where the hump occurs.

The two channel data show scaling with an argument $(eV/k_BT)^1/2$ in agreement with conductance measurements on clean point contacts. It has to be pointed out, though, that this scaling as well as the scaling in the one channel model is only approximate. Finite T–corrections are observed in the numerical data (but also in the experimental data) for temperatures down to about $1/100\,T_K$.

I also calculate the dynamic and static susceptibility and discuss the modifications due to a finite bias by example of the two channel model. The dynamic susceptibility approaches a finite step as $T \to 0$, leading to a logarithmic divergence of the static susceptibility in this limit. A finite bias cuts off this logarithmic divergence. In a very similar fashion, the temperature cuts off the divergence as the bias is vanishing. Differences in the bias and temperature dependence of the static susceptibility appear at high bias and temperature (outside of the scaling regime).

CHAPTER 8
PART II: NONMAGNETIC IMPURITIES IN HIGH T_c SUPERCONDUCTORS

For the high–T_c SC's there is mounting evidence [51] that the superconducting state involves pairing of electrons in a d–wave state rather than an isotropic s–wave state, Fig. 8.1. The most direct evidence is obtained through angle–resolved photo emission spectroscopy (ARPES) which shows a gap with four–fold symmetry and minima (nodes within the experimental resolution) at the lattice diagonals [52]. This is in agreement with $d_{x^2-y^2}$ symmetry of the pair wave function.

Because this state has nodes of the quasiparticle excitation gap Δ_k, the density of states (DOS) is in fact gapless: It grows linearly from the Fermi level and is vanishing only right at the Fermi energy, see Fig. 8.2. This is in contrast to a classic SC with a nonvanishing gap everywhere on the Fermi surface, where the DOS has a gap $2\Delta(T)$ about the Fermi energy.

The presence of nonmagnetic impurities in an otherwise pure d–wave SC has qualitatively different effects compared to their s–wave counterparts. In classic isotropic s–wave SC's nonmagnetic impurities (that is, pure potential scattering) leaves the SC completely unaffected as long as the impurity concentration is low and the scattering strength is small compared to the Fermi energy. This is known as Anderson's theorem [53]: instead of pairing between free electron (or Bloch) states there is pairing of scattering states. Since the impurities are nonmagnetic

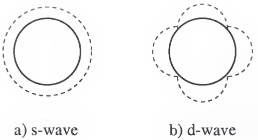

Figure 8.1: a) Isotropic s–wave, and b) $d_{x^2-y^2}$–wave gaps of a superconductor. The solid lines show the cylindrical Fermi surface. The dashed lines indicate the gaps in the quasiparticle excitations. Observe the nodes along the diagonals in the d–wave state.

they cannot break the spin singlet pairs of such states. It takes magnetic impurities to achieve this; the spin flip scattering of electrons on magnetic impurities destroys the singlet pairing. The consequences are e.g. a strong suppression of T_c upon doping with such impurities.

In a d–wave SC even nonmagnetic impurities are pair breaking due to the nodes of the gap on the Fermi surface. This has been shown via self–consistent t–matrix approximation (SCTMA) [54, 55] and very recently also by nonperturbative methods [56]. The effect on the DOS is a further 'filling in' of states in the pseudogap, as shown by the solid line in Fig. 8.2.

Theories based on this picture of a d–wave superconductor with nonmagnetic impurities [57, 58] have been qualitatively successful [59] in explaining properties directly related to the DOS, like the low temperature London penetration depth, specific heat etc. [60–63] However, they fail to describe the low temperature transport properties correctly. Among the more prominent examples for this failure is the low temperature behavior of the microwave conductivity [64,65].

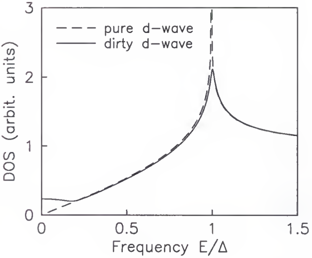

Figure 8.2: Density of states (DOS) of a d–wave superconductor. The dashed line shows the linear behavior of the DOS of a pure superconductor at low energies. The solid line shows the strong modification due to nonmagnetic impurities. Observe that in the 'dirty' case the DOS is finite at the Fermi level.

Experiments measure a linear T–dependence for small concentrations of dopants, e.g. Zn impurities in YBaCuO. This is in contrast to the quadratic behavior found in the simple theories described above. It is possible that this is due to the fact that Zn–impurities in YBaCuO are actually magnetic, so that the result for nonmagnetic impurities does not apply. However, the fact that for a system with nodes like a d–wave SC already nonmagnetic impurities are pair breaking eliminates the big, qualitative difference between nonmagnetic and magnetic impurities present in the classic SC's. One suspects that the qualitative difference present in classical, fully gapped SC's might be only a quantitative one for a d–wave SC.

This leaves one with a puzzle, adding one more to the many involving the high–T_c materials: If the thermodynamics is qualitatively well described by the picture of a 'dirty' d–wave SC, how come that the transport properties obtained by the same model and techniques fail to agree even qualitatively with experiments? The answer lies in the question itself: Obviously there are elements lacking in the standard treatment when it comes to describe two–particle properties involved in transport, whereas the single– particle properties determining the thermodynamics are properly described.

The objective of the proposed work is to determine whether I can achieve better agreement with the experimental transport data within a phenomenological model of a d–wave SC with potential scattering off nonmagnetic impurities and *additional scattering due to self–consistently determined order parameter perturbations about these impurities.* Such additional scattering can be expected to have small effect on single particle properties, since the scattering is off–diagonal in particle-hole space. Transport properties, on the other hand, are much more sensitive to new terms in the quasiparticle scattering rate arising from this new source of scattering. It is therefore plausible that this mechanism can do the trick of affecting only the properties which are up to now not explained within the simplest theories of a dirty d–wave SC.

In the following I will briefly review the current evidence for d–wave superconductivity in the high–T_c SC's. I will also review the problems with transport properties by example of the microwave conductivity. I then introduce the standard treatment of a pure and impure superconductor, that is BCS–theory [66]

and the SCTMA of nonmagnetic impurities. The validity of this approximation has been questioned [67] for a strictly two–dimensional d–wave SC. Therefore, in chapter 11 I discuss a nonperturbative method to treat disorder in a two–dimensional SC which shows that the SCTMA gives at least the qualitatively correct physics.

The main idea of this part of the thesis is the importance of order parameter perturbations about the impurities. I will review the results for s–wave SC's and discuss the differences to order parameter perturbations in a d–wave SC. Then I will discuss the derivation of a new T–matrix for scattering off δ–function impurities with additional scattering due to order parameter perturbations. The knowledge of an analytical form of the T–matrix allows for the self–consistent determination of the order parameter perturbations $\delta\Delta_k(q)$. Using the SCTMA to deal with finite impurity concentrations I then obtain the density of states and the now momentum dependent scattering rate. These results will then be used to compute the microwave conductivity. The thesis will end with conclusions.

CHAPTER 9
D-WAVE PHENOMENOLOGY FOR THE HIGH-T_c SUPERCONDUCTORS

The evidence for pairing in a d–wave state (most likely $d_{x^2-y^2}$) can be roughly categorized in three groups

- Direct probes of the order parameter itself.
- Thermodynamic properties, i.e. properties directly derived from the quasi-particle density of states $N(\omega)$..
- Transport properties, i.e. two-particle properties.

The first two groups are reviewed in detail in Ref. [51], the third group is elaborately discussed in Refs. [59,64]. I will briefly review the main arguments of these papers.

9.1 Direct Probes of the Order Parameter Itself

ARPES measures essentially the occupied part of the angle and energy resolved spectral function $A(\vec{k},\omega)$. The measurements [52] are taken just above T_c for the normal state and well below T_c to measure the fully developed gap in the superconducting state. The gap is determined by the difference of the "Fermi level", that is the threshold between occupied and unoccupied states, of the normal and superconducting states. It has turned out, that this gap is angle dependent in the bismuth– (BSSCO) and yttrium– (YBCO) based high–T_c SC's,

with maxima along the direction of the lattice vectors of copperoxide layers and **nodes** (as far as the resolution of 3–5 meV of the experiments can tell) along the diagonals. This is in agreement with the gap of a pure $d_{x^2-y^2}$–state and in conflict with both isotropic or extended s–wave states (or combination of the mentioned states). In principle, the finite resolution of the experiments allows for an additional isotropic s–wave component of the order parameter. However, the experiments show clearly that if such a component exists, it must be very small, so that it would have impact on thermodynamic and transport properties only at extremely low temperatures.

Magnetic flux measurements (for a review see [51]) are able to determine phase differences of the order parameter on specially manufactured Josephson junctions. The crystals can be grown such that the grain boundaries occur along special direction of the orthorhombic lattice, e.g. the a–direction of one grain has a boundary with the b–direction of the adjacent grain. Several geometries have been studied by several groups [68–71]. The experiments show that there is a phase shift of π between the order parameters of the grains aligned as described above. This implies that there is a relative minus sign of the order parameter along the a– and the b–directions. As a consequence magnetic vortices have been observed which are quantized in halfs of the flux quanta $\phi_o = h^2/ec$. Such vortices have actually been 'seen' by imaging techniques using scanning SQUID microscopes. These observations are again in agreement with a $d_{x^2-y^2}$–pairing state, but can not be explained by neither an isotropic nor an extended s–wave order parameter (no relative minus sign between a– and b– directions).

9.2 Thermodynamic Properties

The thermodynamic properties are essentially determined by the quasi–particle density of states $N(\omega)$. As discussed in the previous chapter, the d–wave and extended s–wave pairing states show linear dependence for $N(\omega)$ in the pure systems, in contrast to the fully gapped $N(\omega)$ of an isotropic s-wave state or a combination of a significant isotropic s-wave component and a d–wave state. A gap in $N(\omega)$ wil lead to activated (exponential) behavior of properties like the specific heat and the London penetration depth. However, gapless systems will show characteristic power laws.

Measurements of the London penetration depth [60, 61] indeed show linear temperature dependence on clean samples as expected from the pure d–wave or extended s–wave pairing states, in strong contrast to the exponential behavior of an isotropic s-wave state. Even more convincing, upon doping with Zinc impurities, the deviation from the $T = 0$– London penetration depth of the clean sample is finite and increases quadratically with temperature at low temperatures. This is in complete agreement with the formation of a finite $N(\omega = 0)$, as expected from a gapless system like d–wave or extended s–wave, in the presence of nonmagnetic impurities (see chapter above). An isotropic s–wave SC would be unaffected my nonmagnetic impurities (Anderson's theorem), so a change of power law is not comprehensible with this pairing state (even if one somehow could explain the power law for the pure system in the first hand).

Specific heat measurements have been more difficult because of the large phononic contribution that dwarfs the electronic part everywhere. Only at the

phase transition does the electronic show up as a minor blimp added to the overall T^3 increase due to the phonons. Recently, several experiments [62, 63] with twinned and untwinned crystals have been able to subtract the phononic contribution by careful comparison to reference samples. They claim that there are both linear and quadratic contributions to the specific heat C in zero magnetic field. In an applied field H, $C \propto H^{1/2}$. Both the quadratic temperature dependence and the square root dependence on the magnetic field are in nice agreement with an order parameter with nodes, like a d–wave or extended s–wave SC [72]. An isotropic s–wave SC, in the other hand, will show activated (exponentially suppressed) behavior in the T–dependence, due to the finite gap in the quasiparticle DOS. For such a SC the magnetic contribution to the specific heat comes excitations localized in the core of magnetic vortices. The number of the vortices is $\propto H$, therefore the resulting specific heat would be also $\propto H$, in contrast to the experiments.

The linear frequency dependence of the DOS of the order parameters with nodes can explain the quadratic contribution but fails to explain the linear contribution in the very clean (nominally pure) samples. The fact that untwinning of the samples strongly effects the coefficient of the linear term but barely effects the quadratic term or the field dependence suggests that the linear term might not be related to the question of order parameter symmetry at all. There are speculations that the linear term could be due to Two–Level–Systems located *between* the copperoxide planes, which would probably not affect the experiments probing the in–plane penetration depth or transport. Still, the linear term is an

open question that needs to be resolved before the case can be closed in favor of the order parameters with nodes.

I conclude that the thermodynamics of pure and impure high–T_c SC's follows naturally from the assumption of a d–wave or extended s–wave pairing state, but is in stark contrast to isotropic s–wave pairing. However, thermodynamic properties cannot distinguish between d–wave or extended s–wave pairing due to the identical density of states $N(\omega)$.

9.3 Transport Properties

Transport properties are the most indirect measure of the order parameter. Nevertheless, because of fact that they also probe the relaxation time in addition to the DOS they also have the potential to bring out the differences between otherwise similar states. As with the thermodynamic properties, studies [59, 64, 65] of the microwave conductivity $\sigma(T)$ of SCs with nonmagnetic impurities have been able to obtain rough agreement with an order parameter with nodes of the d–wave or extended s–wave type. These studies also have shown that admixtures of an isotropic s–wave component must be very small to be permitted by the experimental data. However, especially the low temperature data are not in good qualitative agreement even with a d–wave SC. $\sigma(T)$ rises linearly with temperature in experiments with small doping of Zc-impurities, rather than quadratic as the simplest theories for $\sigma(T)$ in a dirty d–wave SC predict [59]. Although these theories use a phenomenological model of inelastic scattering to account for the downturn of $\sigma(T)$ at temperatures closer to T_c, it is hard to

believe that the inaccuracy in the treatment of inelastic scattering could account for discrepancies in the low temperature regime.

It is therefore reasonable to assume that the standard treatment of the elastic scattering off the nonmagnetic impurities is not quite right. I have investigated the possibility that additional scattering due to impurity–induced order parameter perturbations can have significant impact for the transport properties in SC's with nodes.

CHAPTER 10
BCS-HAMILTONIAN AND T-MATRIX FORMULATION

The theory of impurities in a superconductor rests on two cornerstones of condensed matter theory, namely the BCS–theory [66] of superconductivity and the self–consistent Green function treatment of impurity scattering introduced by Abrikosov and Gor'kov [73]. To clarify notation and as an introduction I will give a brief overview of the physics involved.

10.1 BCS–Theory of Superconductivity

In the classic SC's the formation of pairs of electrons (the Cooper pairs) is a result of an instability of the Fermi sea in the presence of the retarded electron–phonon interaction. If the interaction is weak, BCS–theory (a mean field theory) gives a good description of the physics. In high–T_c SC's, although there are plenty of suggestions, the underlying pairing mechanism is not known. However, consensus has it that phonons play only a minor role in bringing about superconductivity. Spin fluctuations but also mechanisms involving charge degrees of freedom are seriously considered. In these cases the basic energy scale ω_o is of the order of the Fermi energy ϵ_F, rather than the Debye frequency ω_D involved in phononic mechanisms. This change in energy scale allows (in principle) for the high T_c's observed without the necessity of strong pair interactions V, since within BCS $T_c = 1.14\,\omega_o \exp(-1/|N_oV|)$. (It is questionable, though, that ω_o and V are

independent parameters in reality, as experience with phonon mediated superconductivity shows.) It is therefore plausible to use the weak-coupling BCS–theory rather than the much more involved strong coupling Eliashberg–theory [74] for the description of superconductivity, at least as a starting point.

BCS–theory is based on the BCS hamiltonian, a hamiltonian in which a four–fermion interaction has been replaced by the interaction of the quasiparticles with a self–consistently determined mean field Δ_k, the order parameter. It is convenient to use the Nambu–spinor [75] $\Psi_k^\dagger = \left(c_{k,\uparrow}^\dagger, c_{-k,\downarrow}\right)$ and its hermitian conjugate in order to simplify the treatment of both (quasi)–particle and hole degrees of freedom. The c– operators are standard second quantized fermionic operators. In terms of the Nambu–spinors the BCS–hamiltonian of a pure, bulk superconductor reads (τ_i are the Pauli–matrices acting on the Nambu–spinors):

$$H_{BCS} = \sum_k (\epsilon_k - \mu)\Psi_k^\dagger \tau_3 \Psi_k + \sum_{k,q} \Delta_k(q)\Psi_{k+q/2}^\dagger \tau_1 \Psi_{k-q/2} \tag{10.1}$$

where $k = (p+p')/2$ is the Fourier transform of the relative coordinate $r = x_1 - x_2$ of two interacting electrons and $q = p' - p$ is the Fourier transform of the center of mass $R = (x_1 + x_2)/2$. Without loss of generality for my purposes I have assumed a real order parameter $\Delta_k(q)$ in the above hamiltonian.

Since the hamiltonian is bilinear, the corresponding Green function can be evaluated and has the simple form (for Matsubara frequencies $\omega_n = \pi T(2n+1)$ at a given temperature T; I drop the index n whenever possible)

$$\hat{G}_o(k, i\omega) = (i\omega_n \tau_o - \xi\tau_3 - \Delta_k \tau_1)^{-1} \tag{10.2}$$

Observe that due to the Pauli matrices the Matsubara Green function is itself a 2×2 matrix. I denote this by the hat. The theory becomes self–consistent upon imposition of the gap equation, i.e. the requirement, that the order parameter Δ_k is itself an expectation value of a pair of electrons. In general, the gap equation reads

$$\Delta_k(q) = -T \sum_{\omega} \sum_{k'} V_{k,k'} \mathrm{Tr} \left\{ \frac{\tau_1}{2} \hat{G}_o(k' + q/2, k' - q/2, i\omega) \right\}. \tag{10.3}$$

The tracing of the product $\frac{\tau_1}{2}\hat{G}_o$ ensures that we pick the correct component of the matrix Green function. Observe that the right hand side depends implicitly on Δ_k via the Green function.

For a bulk superconductor without impurities the order parameter is supposedly uniform in space. This means that only the $q = 0$ component of the momentum dependent order parameter is nonzero, $\Delta_k(q) = \Delta_k(q = 0) \equiv \Delta_k$. As a result, the hamiltonian 10.1 can be diagonalized (via a Bogoliubov–transformation) and the excitation spectrum of quasiparticles can be found. It is

$$E_k = \sqrt{\xi_k^2 + \Delta_k^2}, \;\; \xi_k = (\epsilon_k - \mu). \tag{10.4}$$

For a clean isotropic s–wave order parameter $\Delta_k = \Delta_o$ the spectrum E_k has a gap of Δ_o about the Fermi level. Therefore, Δ_k is often named the gap. It is important to distinguish between the maximum of the order parameter Δ_k and the (maybe nonexistent) gap in the excitation spectrum for all anisotropic superconductors. Although related, they are only identical for the isotropic s–wave SC's.

The distinction of s–, extended s–, p– (e.g. superfluid ^3He), and d–wave order parameters comes solely from the pairing potential $V_{k,k'}$ as can be seen from the gap equation 10.3. For simplicity, I use a pairing interaction which factorizes in the momentum variables k, k':

$$V_{k,k'} = \sum_l V_l \Phi_l^*(k) \Phi_l(k') \tag{10.5}$$

The index $l, l = 0 \ldots \infty$ indicates the angular momentum "quantum number" of the pair wave function, whereas $\Phi_l(k)$ is a corresponding normalized basis function. The pairing interactions V_l are taken to be independent of the magnitude of k for energies within the interval $[-\omega_o, \omega_o]$ about the Fermi level, and zero otherwise. This is another approximation of the weak coupling BCS–theory. The selection of an order parameter with a specific symmetry is achieved by setting all V_l to zero but the desired one. For example, $d_{x^2-y^2}$–wave superconductivity is achieved by taking $V_2 = V$ as the only nonzero coupling. As a convenient choice for the basis function for a cylindrical Fermi surface in two dimensions one can choose $\Phi_2(k) = \sqrt{2}\cos(2\phi_k)$, where ϕ_k is the angle of the momentum k to the x–axis. Because of the momentum factorization of the pairing interaction the k–dependence of the right hand side of the gap equation can be pulled out of the sums. It follows that the order parameter $\Delta_k = \Delta_{\phi_k}$ will have the same angle dependence as the chosen basis function. This holds even in the case of a nonuniform gap in the case of an impure superconductor.

With a separable pairing interaction of the form above, I can partially perform

the momentum sum leading to (for the d–wave case, $\Delta_k = \Delta \cos 2\phi_k$)

$$1 = -2TVN_o\pi \sum_\omega \int \frac{d\phi_k}{2\pi} \cos^2 2\phi_k \frac{1}{(\omega^2 + \Delta_{\phi_k}^2)^{1/2}} \tag{10.6}$$

The sum over Matsubara frequencies is constraint by $[-\omega_o, \omega_o]$, since the pairing potential vanishes otherwise. N_o is the density of states at the Fermi level of the normal state.

One obtains T_c from the Eq. 10.6 by setting $\Delta_k = 0$. The result is identical to the one quoted above, with $V = V_2$. The temperature dependence of Δ_k is also identical to the standard s–wave case; however, the value at $T = 0$ is $\Delta_k(T = 0) = 2.14T_c\Phi_2(k)$ for d–wave, rather than $\Delta_k(T = 0) = 1.76T_c$ for the s–wave case. The density of states follows from the order parameter and the explicit form of the Green function Eq. 10.2 since

$$N(\omega) \equiv -\frac{1}{\pi} \mathrm{Im} \sum_{\vec{k}} G_{11}(\vec{k}, i\omega \to \omega + i\epsilon) \tag{10.7}$$

where G_{11} is the upper left element of the matrix Green function $\hat{G}$. For a clean $d_{x^2-y^2}$–wave or extended s–wave order parameter $N(\omega)$ is linear at low frequencies as shown in figure 8.2. These types of superconductors are therefore gapless even in the clean limit. The linear frequency dependence of $N(\omega)$ is reflected in low temperature thermodynamic properties like the London penetration depth $\lambda(T)$.

10.2 Self–Consistent T-Matrix Approximation

The self–consistent T-Matrix approximation (SCTMA) is actually not a defi-

nite approximation but rather a term given to the type of approximations in which the T–matrix (defined below) of a single impurity problem is made self–consistent in order to treat low concentrations of impurities for which one expects the single impurity scattering to be dominant over complicated multi–impurity scattering processes. Its validity for three dimensional systems is well established. For the layered high–T_c SC's, for which one might expect two–dimensional physics to be relevant, the applicability of the SCTMA has been challenged [67] for the cases with order parameter nodes. I will argue in the next chapter that for realistic disorder in a two–dimensional d–wave SC the SCTMA gives in fact qualitatively correct results. It is therefore safe to use the SCTMA as long as one bears in mind that certain constants might need experimental input rather than being determined by the theory itself from microscopic parameters. However, qualitative physics like the question of power laws can be addressed by the SCTMA.

Consider nonmagnetic impurities in a bulk superconductor described by the Green function $\hat{G}_o$, Eq. 10.2. Static impurities (potential scatterers) are described by the hamiltonian

$$\begin{aligned} H_{imp} &= \int d^D x \Psi^\dagger(x) U(x - R_{imp}) \tau_3 \Psi(x) \\ &= \sum_{p,p'} \Psi^\dagger(p) U(p,p') \tau_3 \Psi(p') \end{aligned} \tag{10.8}$$

where $U(x - R_{imp})$ is the scattering potential of a impurity located at R_{imp}, and $U(p,p')$ is its Fourier transform. Due to the impurity the full Green function $\hat{G}$ will be nonuniform and therefore depend on two momenta p, p'. Since the impurity is static (it cannot absorb or emit energy) $\hat{G}$ will still be a function of a

single frequency ω. If the impurity is local, that is $U(x - R_{imp}) = U_o\delta(x - R_{imp})$, a Dirac δ–function in space, the full Green function still has nontrivial momentum dependence, however, the irreducible self energy will be a function of frequency alone if certain multi–impurity scattering processes are neglected (irreducible means that no diagrams are allowed that separate into two disconnected pieces upon cutting a single electron line, see below). In general, the self energy $\hat{\Sigma}$ is defined via Dyson's equation

$$\hat{G}(\omega, p, p') = \hat{G}_o(\omega, p)\delta_{p,p'} + \hat{G}_o(\omega, p)\hat{\Sigma}(p, \omega)\hat{G}(\omega, p, p') \tag{10.9}$$

In practice, the self energy is computed via a perturbation expansion. The

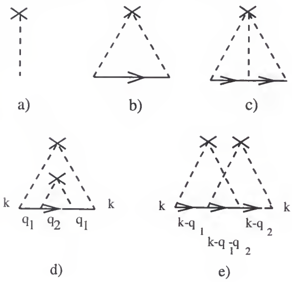

Figure 10.1: Lowest order irreducible self energy diagrams for scattering off local impurities. The cross stands for the impurity, dashed lines indicate the interactions and solid lines represent the electrons. a), b) and c) correspond to scattering off a single impurity. d) and e) are diagrams corresponding to two impurity scattering.

lowest order irreducible diagrams are shown in Fig. 10.1. The cross stands for the impurity, dashed lines indicate the interactions and solid lines represent the quasiparticles. The first diagram is a constant and can be absorbed in the chemical potential. The second diagram corresponds to the second order Born approximation. Such an approximation can be only justified for small interaction potential U. For U of the order of the Fermi energy higher order diagrams, e.g. Fig.10.1 c), become important and have to be accounted for.

This can be done elegantly with the introduction of the T-matrix. In the special case of a single δ-function scatterer the T-matrix has a simple form and can be determined as follows: The T–matrix is defined by the equation

$$\hat{T}(\omega, p, p') = \hat{U}(p, p') + \sum_{p''} \hat{U}(p, p'')\hat{G}_o(i\omega, p'')\hat{T}(\omega, p'', p') \tag{10.10}$$

where $\hat{U}(p, p') = U(p, p')\tau_3$. For a δ–function potential $U(p, p') = U_o$ is a constant. It is intuitively clear (and can be shown rigorously) that the T–matrix can have no momentum dependence, $\hat{T}(\omega, p, p') = \hat{T}(\omega)$. The momentum sum over p'' can therefore be performed and leads to

$$\hat{T}(\omega) = U_o\tau_3 + U_o\tau_3\hat{g}_o(i\omega)\hat{T}(\omega) \tag{10.11}$$

where $\hat{g}_o(i\omega) = \sum_p \hat{G}_o(i\omega, p)$ is the momentum integrated Green function of the bulk SC. For a general SC, the solution is

$$\hat{T}(\omega) = U_o\tau_3(\tau_o - U_o\tau_3\hat{g}_o(\omega))^{-1} \tag{10.12}$$

with τ_o the 2×2 identity matrix. For a d–wave SC the angular integral of the off-diagonal component in $\hat{g}_o(\omega)$ vanishes. The T-matrix then has the particularly simple form

$$\hat{T}(\omega) = \frac{g_o(\omega) U_o^2 \tau_o + U_o \tau_3}{1 - g_o^2(\omega) U_o^2} \; , \tag{10.13}$$

that is, there is no off-diagonal component in the T-matrix itself. In terms of the T-matrix, the full Green function is given by

$$\hat{G}(i\omega, p, p') = \hat{G}_o(i\omega, p)\delta_{p,p'} + \hat{G}_o(i\omega, p)\hat{T}(\omega)\hat{G}_o(i\omega, p') \tag{10.14}$$

As advertised, the Green function still strongly depends on the momenta although neither the self energy nor the T-matrix do so.

Rather than a single impurity I am interested in a low concentration of impurities in a bulk sample. The concentration must be low enough so that multi–impurity scattering processes are unimportant compared to scattering off a single impurity site. One does not expect the actual configuration of impurities to be of any importance in a macroscopic sample. Therefore, I have to average e.g. the self energy diagrams over all possible configurations of impurities. Details of this straightforward procedure can be found e.g. in the article of Ambegoakar in Parks' book on superconductivity [76]. The basic result is that the disorder averaged self energy and the T-matrix are simply related (for δ–function scatterers only) by

$$\hat{\Sigma}(\omega) = n_i \hat{T}(\omega) + \text{crossed diagrams} \; , \tag{10.15}$$

n_i being the impurity concentration. In a three dimensional system, due to phase

space constraints the crossed diagrams obtain a factor $1/(k_F l)$ compared to the uncrossed diagrams, with k_F the Fermi wave number and l the elastic mean free path. Since typically for dilute concentrations of impurities $k_F l \gg 1$ the crossed diagrams can be neglected. In a two dimensional system there is no such a priori suppression of the crossed diagrams. However, as I will show in the next chapter, it still makes sense to neglect the crossed diagrams, since the qualitatively correct behavior is reproduced by this approximation.

The crucial point in Eq. 10.15 is that the T-matrix has the structural form of a single impurity T-matrix, like the one of Eq. 10.13. However, the g_o in it is not the one obtained from the bare (noninteracting) Green function but rather from the Green function with self energy $\hat{\Sigma}(\omega)$. This means that Eq. 10.15 is actually a self–consistency equation for the disorder averaged (momentum independent) self energy $\hat{\Sigma}(\omega)$.

The full solution of Eq. 10.15 is usually only numerically accessible, although important analytical results can be obtained in certain parameter regimes, e.g. for small frequency ω. Having obtained the self energy, one can determine the DOS and from there the thermodynamics of the system. Within linear response, one can also obtain information about the electronic contributions to transport properties like conductivity and thermal conductivity.

CHAPTER 11
VALIDITY OF T-MATRIX APPROXIMATION IN 2D

11.1 General Problem

Recently, Nersesyan et al. [67] have questioned the validity of the SCTMA when applied to a strictly two–dimensional disordered d-wave SC. They pointed out that in 2D no small factors like $1/(k_F l)$ distinguish between uncrossed and crossed diagrams. In fact, straightforward computation shows that the lowest order crossed diagram Fig.10.1 e) (for outer momentum $k = 0$) is of the same order as the corresponding uncrossed diagram Fig.10.1 d) that is accounted for within the SCTMA, namely $\sim \omega^2 \log^2(\Delta/\omega)$ (Δ being the maximum of the order parameter). This is only true for outer momentum $k = 0$, since finite k cut off the logarithmic 'divergence' at low frequencies for the crossed diagram. On the other hand the uncrossed diagram is momentum independent since the integrations over the inner momenta q_1, q_2 are completely independent of k. Although this caveat shows that even in 2D crossed and uncrossed diagrams are not on equal footing, it is clear that one can not neglect the uncrossed diagrams without establishing at least qualitatively in an independent way that such an approximation is justified.

Nersesyan et al. avoided perturbation theory by applying bosonization techniques together with the replica trick. They found a power law DOS $N(\omega) \sim |\omega|^\alpha$, $\alpha \simeq 1/7$, for sufficiently small frequency ω and weak disorder, rather than the

analytic behavior $N(\omega) \sim const + a\omega^2$ expected within SCTMA. Their calculation supports their claim that the uncrossed diagrams should not be neglected, and that the SCTMA breaks down for a two–dimensional d–wave SC. Although the physical systems in question are in reality highly anisotropic 3D systems, the possibility of a 2D-3D crossover at low temperatures could conceivably invalidate some of the results of the usual "dirty d-wave" approach using the SCTMA. This would render the description of the low-temperature transport properties of the cuprate superconductors considerably more complicated even were the order parameter of the simple 2D $d_{x^2-y^2}$ form usually assumed.

In contrast, I show [56] that for certain types of disorder, *exact* results can be obtained for the DOS of strictly 2D disordered superconductors. I show that for *any* disorder diagonal in position and particle-hole space, the DOS of a classic isotropic s-wave superconductor has a rigorous threshold at the (unrenormalized) gap edge Δ, as expected from Anderson's theorem [53]. Within the same general method, I show that the residual DOS $N(0)$ of a superconductor with nodes (e.g. d- or extended s-wave) is nonzero for arbitrarily small disorder. These findings are in disagreement with Ref. [67] but do agree qualitatively with the results of the SCTMA for that system and dimension. Therefore, I conclude that the SCTMA is a valid method to qualitatively describe the considered system and may be used to obtain information on transport properties.

Nersesyan et al. also argued that a non-zero DOS at $\omega = 0$, a quantity indicating spontaneous symmetry breaking, may not occur in a 2D system because of the Mermin-Wagner theorem [77]. I believe that the DOS in a disordered system

is not an order parameter which belongs to the class of order parameters covered by the Mermin–Wagner theorem. This is supported by the fact that a non-zero DOS occurs also in other tight-binding models (e.g., model for two-dimensional Anderson localization [78]), which are described by a field theory with continuous symmetry.

11.2 Superconductor on a Lattice with On-Site Disorder

The method of calculating exactly the DOS of a superconductor for certain types of disorder is motivated by the analysis of Dirac fermions in 2D [79]. The BCS Hamiltonian in first quantized form is given by ($\hbar^2/2m = 1$)

$$H = (-\nabla^2 - \mu)\tau_3 + \hat{\Delta}\tau_1 \ . \tag{11.1}$$

It describes quasiparticles in the presence of the spin singlet order parameter $\hat{\Delta}$. As before, the τ_i are the Pauli matrices in particle-hole (Nambu) space. The disorder is modeled by taking the chemical potential $\mu = \mu_x$ as a random variable distributed according to a probability distribution $P(\mu_x)$.

I consider a 2D square lattice spanned by the unit vectors $\hat{e}_1$ and $\hat{e}_2$. The kinetic energy operator $-\nabla^2$ is defined by its action on a wave function $\Psi(x)$.

$$\nabla^2\Psi(x) = \Psi(x + 2\hat{e}_1) + \Psi(x - 2\hat{e}_1) + \Psi(x + 2\hat{e}_2) + \Psi(x - 2\hat{e}_2) \ . \tag{11.2}$$

This definition involves displacements of two lattice sites rather than one, as would be the case in the simplest tight-binding representation of the lattice kinetic

energy. The reason for this choice is technical convenience at a later part of the calculation. For a system of fermions in the thermodynamic limit, the kinetic energy will have a band representation quite similar to the usual tight-binding form. In particular, there will be no distinguishing features of the band structure near the Fermi level. The definition obeys, of course, the same global continuous symmetries discussed for the model in Ref. [67].

The bilocal lattice operator $\hat{\Delta} \equiv \Delta_{x,x'}$ is taken to act as a c-number in the isotropic s-wave case,

$$\hat{\Delta}\Psi(x) = \Delta\Psi(x), \tag{11.3}$$

whereas to study extended (nonlocal) pairing I define

$$\hat{\Delta}^{s}_{d}\Psi(x) = \Delta^{s}_{d}[\Psi(x+\hat{e}_1) + \Psi(x-\hat{e}_1) \pm \Psi(x+\hat{e}_2) \pm \Psi(x-\hat{e}_2)]\,. \tag{11.4}$$

These are the standard representations of the corresponding order parameters on a square lattice.

I consider the single-particle Matsubara Green function defined as $G(i\omega) = (i\omega\tau_0 - H)^{-1}$ (suppressing the index on the Matsubara frequencies ω_n). I am interested in calculating the DOS

$$N(\omega) \equiv -\frac{1}{\pi}\mathrm{Im}\langle G_{11}(x, x, i\omega \to \omega + i\epsilon)\rangle \tag{11.5}$$

where $\langle ... \rangle$ denotes the disorder average. The major problem is how to perform this disorder average over the probability measure $P(\mu_x)d\mu_x$ of the random variable μ_x. Exact results for the disorder-averaged Green function in noninteracting

systems can frequently be obtained for Lorentzian disorder, by exploiting the simple pole structure of $P(\mu_x)$ in the complex μ_x plane.

$$P(\mu_x)d\mu_x = \frac{(\gamma/\pi)}{(\mu_x - \mu_0)^2 + \gamma^2} d\mu_x \,, \tag{11.6}$$

μ_0 is the chemical potential of the averaged system. For convenience, I set $\mu_0 = 0$. The averaged Green function

$$\langle G(i\omega) \rangle \equiv \int \prod_x d\mu_x P(\mu_x) G(i\omega; \mu_x) \tag{11.7}$$

can be easily evaluated *if* G can be shown to be analytic in either the upper or lower μ–half plane.

In a superconductor, the Green function depends on the random variable μ_x via $\mu_x \pm i\omega$. This is a consequence of the particle-hole structure, i.e. the different Pauli matrices multiplying ω and μ_x. Therefore, the averaging of G with respect to Lorentzian disorder is not trivially possible. However, it is possible to reformulate the problem so that G is a sum of terms each of which are analytic in either the upper or the lower complex μ_x plane. This allows then to perform the averaging of the Green function for Lorentzian disorder.

11.3 Isotropic S-Wave Superconductor

Consider first a homogeneous and isotropic s-wave order parameter. The Matsubara Green function may be written $G(i\omega) = -(i\omega\tau_0 + H)(\omega^2 + H^2)^{-1}$. I note that $H^2 = (-\nabla^2 - \mu)^2\tau_0 + \Delta^2\tau_0$ since in the isotropic s-wave case, $(-\nabla^2 - \mu)\tau_3$

anticommutes with $\Delta\tau_1$ even for random μ_x. This is due to the locality of the order parameter $\hat{\Delta}$ in this case.

The expression $H^2+\omega^2\tau_0$ is proportional to the unit matrix; as a consequence, the Green function can be written in the simple form

$$G(i\omega) = -\frac{i\omega\tau_0 + H}{2i\sqrt{\Delta^2+\omega^2}}\left[\frac{1}{-\nabla^2-\mu-i\sqrt{\Delta^2+\omega^2}} - \frac{1}{-\nabla^2-\mu+i\sqrt{\Delta^2+\omega^2}}\right]\tau_0 \tag{11.8}$$

The imaginary part of this expression (after analytic continuation) for *any given configuration of impurities* is vanishing for $|\omega| < \Delta$. Therefore, the DOS shows a gap of size Δ *independent* of the distribution function $P(\mu)$. Thus, the model reproduces the famous Anderson theorem [53] which states that the thermodynamics of an isotropic s-wave superconductor are not affected by diagonal, nonmagnetic disorder. The situation is different if the order parameter itself is random [80, 81]. In that case all quasiparticle states are broadened and the DOS is finite even for the isotropic s-wave SC.

11.4 D- and Extended-S Symmetry Superconductors.

My main concern is with the d-wave and extended-s "bond" order parameters $\hat{\Delta}^{s}_{d}$ defined above. The corresponding pure systems in momentum space fulfill the condition $\sum_k \Delta_k = 0$, so that nonmagnetic disorder must cause significant pair breaking [54]. The behavior of the imaginary part of the Green function can be studied using a method analogous to that used for the s-wave case. However, because of its nonlocal nature the order parameter $\hat{\Delta}^{s}_{d}\tau_1$ does not anticommute

with $(-\nabla^2 - \mu)\tau_3$ anymore if μ is random. As a consequence, H^2 is no longer proportional to the unit matrix τ_0, which forbids a simple separation of poles of the Green function as in the s–wave case, Eq. 11.8. A different type of transformation is required. I introduce a diagonal matrix (or staggered field) $D_{x,x'} = (-1)^{x_1+x_2}\delta_{x,x'}$ (note D^2 is the unit matrix). Now I may write

$$H^2 = HD\tau_3^2 DH = [(-\nabla^2 - \mu)D\tau_0 - i\hat{\Delta}^{s}_{d} D\tau_2][D(-\nabla^2 - \mu)\tau_0 + iD\hat{\Delta}^{s}_{d}\tau_2] \quad (11.9)$$

D commutes with $-\nabla^2$ and μ as defined above, because $-\nabla^2$ involves only next nearest neighbor sites and μ is local. However, D anticommutes with the order parameter $\hat{\Delta}^{s}_{d}$, since the nonlocal order parameter involves nearest neighbor sites. This yields simply $H^2 = \tilde{H}^2$, with

$$\tilde{H} \equiv (-\nabla^2 - \mu)D\tau_0 - i\hat{\Delta}^{s}_{d} D\tau_2 \,. \quad (11.10)$$

Therefore, the quantity $\tilde{H}^2 + \omega^2\tau_0 = (\tilde{H} + i\omega\tau_0)(\tilde{H} - i\omega\tau_0)$ can be used to write

$$G(i\omega) = \frac{i(i\omega\tau_0 + H)}{2\omega}\left(\frac{1}{\tilde{H} - i\omega\tau_0} - \frac{1}{\tilde{H} + i\omega\tau_0}\right) \quad (11.11)$$

Note that both H and $\tilde{H}$ appear in this expression, but H only in the numerator.

Defining $z_x \equiv \mu_x D_{x,x}$, I now note that for $\omega > 0$ *and* $\mathrm{Im}(z_x) \geq 0$ the matrix $i\omega\tau_0 - \tilde{H}$ is non-singular (i.e., $det(i\omega\tau_0 - \tilde{H}) \neq 0$). Therefore, the transformed Green's function $(i\omega\tau_0 - \tilde{H})^{-1}$ can be expanded as a Taylor series with nonzero radius of convergence around any z_x in the upper half $z-$ plane, and is consequently analytic there. Correspondingly, $(i\omega\tau_0 + \tilde{H})^{-1}$ is analytic in the lower

half $z-$ plane. Due to these analytic properties and using $P(z_x) = P(\mu_x)$ I can now straightforwardly perform the disorder integration. Care has to be taken when evaluating the numerator involving H, since it involves μ_x rather than z_x. It turns out, though, that all terms involving the matrix D vanish.

The resulting disorder averaged Matsubara Green function is translational invariant. Performing a spatial Fourier transform I replace $-\nabla^2$ by $\xi = \epsilon_{\vec{k}} - \mu_0$ and obtain

$$\langle G(i\omega)\rangle = -\frac{(i\omega + i\gamma)\tau_0 + \xi\tau_3 + \Delta_d^s\tau_1}{(\omega+\gamma)^2 + \xi^2 + (\Delta_d^s)^2} \equiv G(i\omega + i\gamma)\,. \tag{11.12}$$

This is the Matsubara Green function of the pure system with the frequency $i\omega$ shifted by the disorder parameter, $i\omega \to i\omega + i\gamma$. In contrast, for the local (isotropic) s–wave order parameter discussed before, the average over a Lorentzian distribution in Eq. 11.8 implies a shift $i\sqrt{\Delta^2+\omega^2} \to i\sqrt{\Delta^2+\omega^2} + i\gamma$.

To obtain the DOS for the d–wave case I approximate the sum over the momenta $\vec{k}$ in standard fashion as $N_o \int_{-\infty}^{\infty} d\xi \int_0^{2\pi} \frac{d\phi}{2\pi}$ where N_o is the density of states of the normal metal at the Fermi level. I also approximated the tetragonal Fermi surface of a square lattice by a circle. The result is

$$N(\omega) = N_0 \int_0^{2\pi} \frac{d\phi}{2\pi} \mathrm{Im}\left(\frac{\omega + i\gamma}{(\Delta_d^2(\phi) - (\omega+i\gamma)^2)^{1/2}}\right) \tag{11.13}$$

where the d–wave order parameter is approximated by $\Delta_d(\phi) = \Delta_d \cos(2\phi)$. At $\omega = 0$, this leads to $N(0) = N_0 \frac{2\gamma}{\pi\Delta_d} \ln(4\Delta_d/\gamma)$ for $\gamma << \Delta_d$. Thus, the density of states is nonzero at the Fermi level for arbitrarily small values of the disorder

parameter γ. If I expand the integral for small values of ω, I find that $N(\omega)$ rises as ω^2.

For more general continuous distributions $P(\mu)d\mu$ the averaged DOS can be estimated using again the analytic structure of G. Applying the ideas of Ref. [80], one can derive a lower bound by a decomposition of the lattice into finite sub-blocks. The average DOS on an isolated sub-block can be estimated easily. Moreover, the contribution of the connection between the sub-blocks to the average DOS can also be estimated. A combination of both contributions leads to $\langle N(0)\rangle \geq c_1 \min_{-\mu_1 \leq \mu \leq \mu_1} P(\mu)$, where c_1 and μ_1 are distribution dependent positive constants. In particular, μ_1 must be chosen such that the spectrum of $H(\mu_0 = 0) = -\nabla^2 \tau_3 + \hat{\Delta}^{s}_{d} \tau_1$ is inside the interval $[-\mu_1, \mu_1]$. For all unbounded distributions, like the Gaussian distribution used in Ref. [67], as well as compact distributions with sufficiently large support this estimate leads to a nonzero DOS at the Fermi level.

11.5 Consequences and Comparison to Other Methods.

The major result in the d–wave (extended s–wave) case with Lorentzian disorder is the presence of a finite purely imaginary self–energy $\Sigma_0 = -i\gamma\tau_0$ due to nonmagnetic disorder. This leads to a *nonzero* DOS at the Fermi level, in qualitative agreement with standard theories based on the SCTMA [57, 58] as well as with exact diagonalization studies in 2D [82]. In contrast to such theories the above self energy has no dependence on $\hat{\Delta}^{s}_{d}$, i.e. it is the same as in the normal state. In Fig. 11.1 I show a comparison of the self energies of my theory and the

weak (Born)– and unitary–scattering limits of the SCTMA.

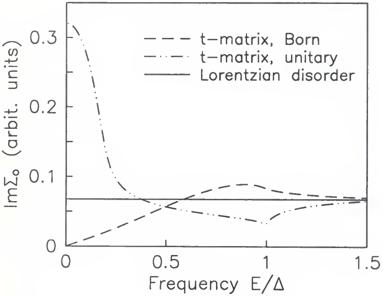

Figure 11.1: Imaginary part of the self energy vs. frequency. For Lorentzian disorder (solid line) the self energy is constant $i\gamma$. The self energy of the self–consistent T–matrix approximation in the unitary scattering limit (dashed–dotted line) behaves $\propto (\Delta\,\delta)^{1/2}$ at zero frequency. For Born scattering (dashed line) the value at zero frequency is nonzero, but exponentially small. I have adjusted the impurity concentration to obtain equal normal state self energies for the T–matrix results.

A drawback of the model with Lorentzian disorder is that impurity concentration does not appear explicitly in the theory. Whereas in the T–matrix approach I have with the impurity concentration and the scattering strength (or phase shift) two parameters associated with disorder, in the present model I have only γ, the width of the Lorentzian. A way of making a connection is by comparing the variance of the Lorentzian distribution (γ) and the variance of the distribu-

tion underlying the T–matrix approximation, which is a bimodal distribution of a chemical potential $\mu = \mu_0$ with probability $1 - \delta$ (δ being the dimensionless impurity concentration) and $\mu = \mu_0 + V$ with probability δ (V being the scattering potential). The variance Var_μ of this distribution is determined by

$$\mathrm{Var}_\mu^2 = \langle \mu^2 \rangle - \langle \mu \rangle^2 = V^2(\delta - \delta^2) \; . \tag{11.14}$$

For small concentrations of impurities, $\delta << 1$, I find $\mathrm{Var}_\mu = V\delta^{1/2}$. The $\delta^{1/2}$ behavior is also found for $\mathrm{Im}\Sigma_o(\omega = 0)$ in the T-matrix approach for strong scattering. Since in my model the variance of the distribution is also the imaginary part of the self energy, this suggests that my model is closer to the strong scattering limit of the SCTMA than the Born limit.

Finally, I comment on the discrepancies between my result and the calculation of Nersesyan et al., who found a power law for the averaged DOS with Gaussian disorder.

One might question the analysis of Nersesyan et al. because of the use of the replica trick, which is a dangerous procedure in a number of models. [83] However, Mudry et al. [84] have obtained identical results for the *continuum* problem of Dirac fermions in the presence of a random gauge field using supersymmetry methods. I therefore believe that the crucial difference between my results and those of Ref. [67] occurs in the passage to the continuum and concomitant mapping of the site disorder in the original problem onto the random gauge field. Only in the continuum case is there a direct analogy between disorder in the chemical potential and a gauge field; on the lattice, gauge fields and chemical

potential terms enter quite differently. First, chemical potential terms are local while gauge fields are defined on bonds. Furthermore, chemical potential disorder enters linearly in the Hamiltonian while gauge fields enter through the Peierls prescription as a phase in the exponential multiplying the kinetic energy.

Disorder of the gauge field type is furthermore nongeneric even in the continuum, as discussed by Mudry et al., who showed that the critical points of the system with random gauge field are *unstable* with respect to small perturbations by other types of disorder. I expect that a proper mapping of the lattice Dirac fermion or d-wave superconductor problems to continuum models will inevitably generate disorder other than random gauge fields. Therefore, I believe that my result of a finite DOS at the Fermi level is the generic case for a d-wave superconductor in two dimensions.

In summary, this calculation suggests that the standard T–matrix approach to disordered d–wave superconductors is qualitatively sufficient. I doubt that the result by Nersesyan et al., who found a power law for the averaged DOS with Gaussian disorder, is of any relevance for the system under consideration.

CHAPTER 12
LOCAL ORDER PARAMETER PERTURBATIONS

Order parameter perturbations in the vicinity of nonmagnetic impurities are present even in the classic s–wave SC's. Fetter [85] has calculated the perturbations about a single impurity within a continuum model in three dimensions, and found that they have the following general behavior: a) They are oscillatory, in analogy to Friedel oscillations of interacting metals, and b) they decay like a power law within a distance of the coherence length ξ and exponentially for distances larger than ξ. A sketch of this behavior is shown in Fig. 12.1. Later,

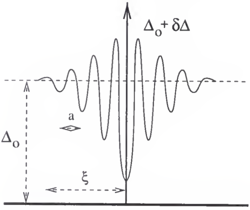

Figure 12.1: Sketch of the order parameter perturbations around a nonmagnetic impurity. The perturbations are oscillatory on atomic lengths scales a and decay exponentially beyond the coherence length ξ. Δ_o is the maximum of the bulk order parameter.

Shiba [86], Rusinov [87] and Schlottmann [88] have worked on various aspects of the problem of magnetic and nonmagnetic impurities in an s–wave SC. Recently,

numerical work has been performed on a model of nonmagnetic impurities on a two–dimensional lattice for both s–wave and d–wave SC's [82, 89].

Despite the above general similarities, there are important differences between the order parameter perturbations of classic s–wave SC's and the high-T_c d–wave SC's. These are:

- The order parameter perturbations are anisotropic, reflecting the d–wave nature of the underlying SC.
- The coherence length ξ is much shorter than in high T_c SC's than in classical SC's, $\xi \sim 10 - 15$Å, which is a few atomic distances.
- The small momentum transfer component of the order parameter perturbations can be large in d–wave SC's, in stark contrast to the isotropic s–wave SC's where it is vanishing.

The first point is not surprising and of minor importance. The short range of the perturbations is helpful since it allows us to treat them as local perturbations around the impurities with no direct interference with perturbations due to other impurities (in the dilute limit). It is the third point, however, which makes all the difference. The fact that the d–wave order parameter Δ_k has zero average when integrated over the Fermi surface leads to a qualitative different behavior of the d–wave SC even in the case of a single impurity. For an s–wave SC the spatial integral of the order parameter perturbations, i.e. the $q = 0$–component, average out to zero, $\delta\Delta(q = 0) \equiv 0$, in agreement with Anderson's theorem. However, for a d–wave SC the order parameter perturbations have a *nonzero* average.

Furthermore, and somewhat counterintuitively, $\delta\Delta(q = 0)$ is not bounded by the bulk gap Δ [90] as I will show below. It is therefore important to determine these perturbations self–consistently via the gap equation. In principle, the gap equation asks for such self–consistency in both s–wave and d-wave cases, but the vanishing of the $\delta\Delta(q = 0)$ without self–consistency implies that the corrections are negligible if self–consistency is taken into account for the s–wave case. I discuss this in more detail below.

12.1 Single Impurity Scattering, Self–Consistent to First Order

For a bulk d-wave SC the (matrix)–Green function reads (Eq. 10.2):

$$\hat{G}_o(k, i\omega) = (i\omega - \xi\tau_3 - \Delta_\phi\tau_1)^{-1}, \tag{12.1}$$

where I assume an order parameter of the form $\Delta_\phi = \Delta\cos 2\phi$. A helpful quantity is the momentum integrated Green function g_o given by

$$g_o(i\omega) = \sum_k \mathrm{Tr}[\frac{\tau_1}{2} G_o(k, \omega)] = -N_o\pi \int_0^{2\pi} \frac{d\phi}{2\pi} \frac{i\omega}{(\Delta_\phi^2 - (i\omega)^2)^{1/2}}. \tag{12.2}$$

Note that there is no off-diagonal part ($\propto \tau_1$) due to the d–wave symmetry. For scattering off a single δ–function impurity with strength U_o I derived in chapter 10 the T-matrix, Eq. 10.13

$$\hat{T}(\omega) = \frac{g_o(\omega)U_o^2\tau_o + U_o\tau_3}{1 - g_o^2(\omega)U_o^2} \ . \tag{12.3}$$

In general, the (weak coupling) gap equation reads (see chapter 10, Eq. 10.3)

$$\Delta_k(q) = -T\sum_\omega\sum_{k'} V_{k,k'}\mathrm{Tr}\left\{\tau_1\hat{G}(k'+q/2,k'-q/2,i\omega)\right\}. \tag{12.4}$$

with $\hat{G}$ now given by $\hat{G} = \hat{G}_o + \hat{G}_o + \hat{G}_o\hat{T}\hat{G}_o$ as in Eq. 10.14. Assuming the pairing potential is separable and has d–wave symmetry ($V_{k,k'} = V\Phi_2(k)\Phi_2(k')$) I can ask for the change of the gap $\delta\Delta_k(q)$ due to the impurity scattering.

$$\delta\Delta_k(q) = -V\Phi_d(k)T\sum_\omega\sum_{k'}\Phi_d(k')\mathrm{Tr}\left\{\frac{\tau_1}{2}\hat{G}_o(k'+q/2,i\omega)\hat{T}(\omega)\hat{G}_o(k'-q/2,i\omega)\right\}. \tag{12.5}$$

This equation determines the order parameter perturbations to zeroth order, in the sense that, although I use the gap equation, I assumed an unperturbed order parameter on the right side of Eq. 12.5. Clearly, this is inconsistent.

Shiba and Rusinov [86, 87] first treated the perturbations self–consistently to first order (for an s–wave SC, for d–wave see [90] and below). They noted that, to first order, it is enough to add a term $\delta T_{k'}(q,\omega)$

$$\delta T_{k'}(q,\omega) = \hat{G}_o(k'+q/2,i\omega)\delta\Delta_{k'}(q)\hat{G}_o(k'-q/2,i\omega) \tag{12.6}$$

to the r.h.s. of Eq. 10.13. This is basically the first term in a perturbation series for the T–matrix with a scattering potential $\delta\Delta_{k'}(q)$. Now both the left and right side of the gap equation are linear in $\delta\Delta_k(q)$. Due to linearity one can separate the terms $\propto \delta\Delta_k(q)$ from the terms not containing $\delta\Delta_k(q)$. For brevity, I consider here only the case $q = 0$, leaving the q–dependent expression to the Appendix C.

Since $\delta\Delta_k(q=0) = \delta\Delta \cos 2\phi_k$ the $k-$ dependence drops out of Eq. 12.5 with the modified T-matrix. The sum over momenta k' is rewritten in standard fashion, $\sum_k' \rightarrow \int \frac{d^2k'}{(2\pi)^2} = N_o \int d\xi \int \frac{d\phi}{2\pi}$, with N_o the normal density of states at the Fermi level. Only few terms survive the tracing procedure and the integration over the energy $\xi = \epsilon_{k'} - \mu$. Explicitly, the equation for $\delta\Delta$ reads

$$\delta\Delta\left(1/V + 2T\sum_\omega N_o \int \frac{d\phi}{2\pi}\cos^2 2\phi \int d\xi \frac{\Delta_\phi^2 - \omega^2 - \xi^2}{(\omega^2 + \xi^2 + \Delta_\phi^2)^2}\right)$$
$$= -2T\sum_\omega N_o \int \frac{d\phi}{2\pi}\cos^2 2\phi \int d\xi \frac{2\Delta i\omega g_o U_o^2}{(\omega^2 + \xi^2 + \Delta_\phi^2)^2}. \tag{12.7}$$

The $\xi-$ integrals are easily computed:

$$I_1 = \int_{-\infty}^{\infty} d\xi \frac{1}{(a^2 + \xi^2)^2} = \frac{\pi}{2a^3}, \quad I_2 = \int_{-\infty}^{\infty} d\xi \frac{\xi^2}{(a^2 + \xi^2)^2} = \frac{\pi}{2a}. \tag{12.8}$$

This yields for Eq. 12.7

$$\delta\Delta\left(1/V - 2T\sum_\omega N_o\pi \int \frac{d\phi}{2\pi}\cos^2 2\phi \frac{\omega^2}{(\omega^2 + \Delta_\phi^2)^{3/2}}\right)$$
$$= -2T\sum_\omega N_o\pi \int \frac{d\phi}{2\pi}\cos^2 2\phi \frac{\Delta i\omega g_o U_o^2}{(\omega^2 + \Delta_\phi^2)^{3/2}}. \tag{12.9}$$

Adding and subtracting Δ_ϕ^2 in the numerator of the integral on the left hand side, I obtain a term

$$C = -2TN_o\pi \sum_\omega \int \frac{d\phi}{2\pi}\cos^2 2\phi \frac{1}{(\omega^2 + \Delta_\phi^2)^{1/2}} \equiv -1/V \tag{12.10}$$

which can be seen by comparing with the gap equation 10.6. The remaining

expressions do not explicitly depend on the coupling V. The final result is

$$\delta\Delta\left(N_o\pi 2T\sum_\omega\int\frac{d\phi}{2\pi}\cos^2 2\phi\frac{\Delta_\phi^2}{(\omega^2+\Delta_\phi^2)^{3/2}}\right)$$
$$= -N_o\pi 2T\sum_\omega\int\frac{d\phi}{2\pi}\cos^2 2\phi\frac{\Delta i\omega g_o U_o^2}{(\omega^2+\Delta_\phi^2)^{3/2}}. \tag{12.11}$$

To get an idea about the order of magnitude of $\delta\Delta$ I consider the Ginzburg–Landau (GL) regime, that is, temperatures close to T_c, so that the order parameter Δ_ϕ is small. I therefore can neglect Δ_ϕ in the denominators of Eq. 12.11. This renders the angular integrals trivial. With the same assumptions I find $g_0 = -iN_o\pi$. I am now in a position to perform the Matsubara sums. The relevant sums are

$$T\sum_\omega 1/|\omega|^3 = c_3/T^2\,,\quad T\sum_\omega 1/\omega^2 = c_2/T\,, \tag{12.12}$$

with dimensionless constants c_2, c_3 that can be expressed in terms of Riemann ζ-functions. Since I am in the GL–regime I replace the temperature T by T_c and find

$$\delta\Delta = -\frac{\frac{(N_o\pi U_o)^2}{1+(N_o\pi U_o)^2}\frac{c_2}{2T_c}}{N_o\pi\frac{3c_3}{8}\frac{\Delta^2}{T_c^2}}\Delta\,. \tag{12.13}$$

A similar result was obtained by Choi and Muzikar [91] in a different context.

12.2 Discussion of the First Order Result

This result has been deceptively written to meet the expectation, namely that $\delta\Delta$ is some negative coefficient times the bulk gap Δ. However, the 'coef-

ficient' is itself inversely proportional to Δ^2. Therefore, $\delta\Delta$ is actually *inversely* proportional to Δ. Since Δ approaches zero as $T \to T_c$ like $(1 - T/T_c)^{1/2}$, $\delta\Delta$ *diverges* like $(1 - T/T_c)^{-1/2}$. This at first hand counterintuitive result could be understood by considering that the $q = 0$ component of $\delta\Delta_k(q)$ is nothing but the total volume integral of the order parameter perturbations. The divergence of $\delta\Delta_k(q = 0)$ therefore signifies that the order parameter perturbations are long ranged. This would be in agreement with the early mentioned general behavior of the order parameter perturbations, namely that their range (after which they decay exponentially) is governed by the coherence length. Since the coherence length diverges as one approaches the critical point so does the range of the order parameter perturbations, and their volume integral therefore diverges.

This argument seems reasonable, however, it neglects that the approximation I used assumed order parameter perturbations to be small, so that I could use the standard T-matrix with a linear correction term. A diverging $\delta\Delta_k(q = 0)$ invalidates the basic assumption. In fact, there is no physical reason why $\delta\Delta_k(q = 0)$ should diverge. The argument above shows that it can be large. Therefore, higher order calculations are indispensable, at least in the unitary scattering limit, $N_o \pi U_o \gg 1$, and close to T_c. My method of incorporating all orders of $\delta\Delta_k(q = 0)$ (see next chapter) leads to a vanishing $\delta\Delta_k(q = 0)$ close to T_c, rather than diverging one. In the other hand, my approximation assumes short ranged order parameter perturbations, an assumption that is clearly violated close to T_c. At the moment, it is unclear to me whether long range effects or higher order corrections dominate close to T_c.

However, I am not really interested in temperatures close to T_c but the effect of the order parameter perturbations on low temperature transport. At low temperatures, the linear approximation is not diverging, but still $\delta\Delta_k(q = 0)$ turns out to be too large to be used with good conscience. I therefore treat $\delta\Delta_k(q)$ properly to all orders. This can be achieved by considering it a new, induced scattering term in the hamiltonian in addition to the standard, direct scattering term of the nonmagnetic impurities. This asks for a completely new determination of the T–matrix. In the next chapter, I will show a way to obtain an *analytical* result for the T–matrix that incorporates the major physics of the new scattering terms.

To conclude this chapter let me stress again the contrast between isotropic s–wave and d–wave SC's when it comes to $\delta\Delta_k(q = 0)$. To linear order one finds that, rather than diverging in the GL–limit, the order parameter perturbations $\delta\Delta_k(q = 0) \equiv 0$ for all temperatures. This is because for an s–wave SC there is an off–diagonal term ($\propto \tau_1$) in the momentum integrated Green function $\hat{g}_o$. This term turns out to cancel *exactly* the term on the right hand side of the equivalent of Eq. 12.11. Since the total right hand side of the equation is zero, so must be $\delta\Delta_k(q = 0)$ for all temperatures T. Within my method of calculating $\delta\Delta_k(q = 0)$ to all orders I also find that $\delta\Delta_k(q = 0) = 0$ is a solution to the nonlinear equation, though other solutions might be possible. I therefore believe that for an s–wave SC $\delta\Delta_k(q = 0)$ is either zero or too small to play any relevant role.

CHAPTER 13
A NEW T-MATRIX AND CONSTITUTIVE EQUATION FOR THE ORDER PARAMETER PERTURBATIONS

13.1 General Remarks

It was shown in the last chapter that $\delta\Delta_k(q)$ is not a priori small when compared to the Fermi energy and standard scattering terms. It is therefore necessary to take more than just the first order of $\delta\Delta_k(q)$ into account. This poses a serious problem, since $\delta\Delta_k(q)$ is both anisotropic and q–dependent (nonlocal). Especially the q–dependence makes the problem analytically intractable, since $\delta\Delta_k(q)$ is determined by a nonlinear self-consistency equation. Future work might use either heavy numerical or variational techniques to improve upon this calculation. As a first step, however, I try to obtain approximate results by exploiting the short range of the fluctuations.

The anisotropy (k–dependence) can be handled as soon as the assumption of locality (no q–dependence) is made. Assuming cylindrical symmetry of the Fermi surface I can perform a partial wave expansion of the functions on the Fermi surface, that is, I express them in terms of the coefficients of $\cos l\phi$ and $\sin l\phi$. I assume that only s– and d–wave scattering takes place. This is essentially an assumption about the pairing potential $V_{p,p'}$: If it contains only s– and d–wave components no other terms can be induced. In principle, the technique can be extended to higher partial waves (at least at $q = 0$).

The procedure described first computes an *analytical* form of the (now momentum dependent) T-matrix as a function of parameters characterizing diagonal ($\propto \tau_3$) and off–diagonal ($\propto \tau_1$) $s-$ and d–wave scattering. These parameters can then be determined by use of the gap equation. This can only be done numerically and the results will be shown in the next chapter.

13.2 Determination of the T-matrix

For clarity I repeat the definitions of the Green function and its momentum integral.

$$\hat{G}_o(k,\omega) = (i\omega - \xi\tau_3 - \Delta_\phi\tau_1)^{-1}, \tag{13.1}$$

$$\hat{G}_o(\phi,\omega) = \int d\xi \hat{G}_o(\xi,\phi,\omega) \tag{13.2}$$

$$\hat{g}_l(\omega) = \int_0^{2\pi} \frac{d\phi}{2\pi} \cos l\phi \hat{G}_o(\phi,\omega) \tag{13.3}$$

For a bulk d–wave SC I take $\Delta_\phi = \Delta\cos 2\phi$ from which follows that

$$\hat{g}_o(\omega) = g_o\tau_o = -N_o\pi \int_0^{2\pi} \frac{d\phi}{2\pi} \frac{i\omega}{(\Delta_\phi^2 - (i\omega)^2)^{1/2}} \tau_o, \tag{13.4}$$

$$\hat{g}_2(\omega) = g_2\tau_1 = -N_o\pi \int_0^{2\pi} \frac{d\phi}{2\pi} \frac{\cos 2\phi \Delta \cos 2\phi}{(\Delta_\phi^2 - (i\omega)^2)^{1/2}} \tau_1, \tag{13.5}$$

$$\hat{g}_l(\omega) \equiv 0 \text{ for all } l \text{ odd} \tag{13.6}$$

I also have $\hat{g}_{-l} = \hat{g}_l$. The higher even g_l's can be related to the given ones and are in general suppressed by a factor of $1/l$.

I attempt to find the T-matrix defined by the equation [92]

$$\hat{T}_{p,p'}(\omega) = \hat{U}_{p,p'} + \int_o^{2\pi} \frac{d\phi}{2\pi} \hat{U}_{p,p_1} \hat{G}_o(\phi,\omega) \hat{T}_{p_1,p'}(\omega) \tag{13.7}$$

where ϕ is the angle of p_1 to the x–axis. The momenta (p,p') are pinned at the Fermi surface. $\hat{U}_{p,p'}$ is a general scattering term which can involve diagonal and off–diagonal s– and d–wave scattering. I expand $\hat{U}, \hat{G}_o$ and $\hat{T}$ in the following way (partial wave expansion):

$$\hat{U}_{p,p'} = \sum_{l,l'} \left(\hat{U}^e_{l,l'} \cos l\phi_p \cos l'\phi_{p'} + \hat{U}^o_{l,l'} \sin l\phi_p \sin l'\phi_{p'} \right) \tag{13.8}$$

$$\hat{G}_o(\phi,\omega) = \sum_m \hat{g}_m \cos m\phi \tag{13.9}$$

$$\hat{T}_{p,p'} = \sum_{n,n'} \left(\hat{T}^e_{n,n'} \cos n\phi_p \cos n'\phi_{p'} + \hat{T}^o_{n,n'} \sin n\phi_p \sin n'\phi_{p'} \right) \tag{13.10}$$

Here, the superscripts e/o denote even and odd terms upon reflection on the x–axis, e.g. $\phi_p \to -\phi_p$. Specifically, I choose the $\hat{U}_{l,l'} = \hat{U}_l \delta_{l,l'}$ with

$$\hat{U}^e_o = \hat{U}_o = U_o\tau_3 + \delta_s\tau_1 \qquad \hat{U}^o_o = 0 \tag{13.11}$$

$$\hat{U}^e_1 = \delta_d\tau_1 \qquad \hat{U}^o_1 = -\delta_d\tau_1 \tag{13.12}$$

$$\hat{U}^e_l = \hat{U}^o_l = 0 \quad \text{for all} \quad l > 1 \; , \tag{13.13}$$

leading to

$$\hat{U}_{p,p'} = U_o\tau_3 + \delta_s\tau_1 + \delta_d \left(\cos\phi_p \cos\phi_{p'} - \sin\phi_p \sin\phi_{p'} \right) \tau_1 . \tag{13.14}$$

The choice for $\hat{U}_1$ is motivated by considering a d–wave scattering term like $\delta_d \cos 2\phi_k$. Since $\vec{k} = (\vec{p} + \vec{p'})/2$ I have

$$\delta_d \cos 2\phi_k = \delta_d \left(\cos\phi_p \cos\phi_{p'} - \sin\phi_p \sin\phi_{p'}\right) \qquad (13.15)$$

for forward scattering ($q = |\vec{p} - \vec{p'}| \to 0$). An explicit q–dependence is neglected, since at the moment I am only interested at $q \to 0$.

The integral (I) in Eq. 13.7 can now be performed at the cost of the summations over the partial wave indices (which run over all integers). The result is (suppressing the ω–dependence)

$$\begin{aligned} I = & \sum_{n,n'} \hat{U}_o \hat{g}_n \hat{T}_{n,n'} \cos n'\phi_{p'} \\ & + \frac{1}{4} \sum_{n,n'} \hat{U}_1 \left(\hat{g}_{n+1} + \hat{g}_{n-1} + \hat{g}_{-n+1} + \hat{g}_{-n-1}\right) \hat{T}^e_{n,n'} \cos n\phi_p \cos n'\phi_{p'} \\ & - \frac{1}{4} \sum_{n,n'} \hat{U}_1 \left(\hat{g}_{n-1} + \hat{g}_{-n+1} - \hat{g}_{n+1} - \hat{g}_{-n-1}\right) \hat{T}^o_{n,n'} \sin n\phi_p \sin n'\phi_{p'} \,. \end{aligned} \qquad (13.16)$$

This expression allows me to write a general system of (inhomogeneous) linear equations for the $\hat{T}^{e/o}_{n,n'}$. In the spirit of the choice for the $\hat{U}_1$ I will assume that all $\hat{T}^{e/o}_{n,n'}$ are negligible for $n, n' > 1$. Such a choice is always a solution, though it may not be the only one in a general case. Then only $\hat{g}_o$ and $\hat{g}_2$ enter the equations which read

$$\begin{aligned} \hat{T}_{o,o} &= \hat{U}_o + \hat{U}_o \hat{g}_o \hat{T}_{o,o} \\ \hat{T}^e_{1,1} &= \hat{U}_1 + \hat{U}_1 (\hat{g}_o + \hat{g}_2) \hat{T}^e_{1,1} \end{aligned}$$

$$\hat{T}^o_{1,1} = -\hat{U}_1 - \hat{U}_1(\hat{g}_o - \hat{g}_2)\hat{T}^o_{1,1} \tag{13.17}$$

where I used the $T^e_{-n,n'} = T^e_{n,n'}$, $T^o_{-n,n'} = -T^o_{n,n'}$. All equations for indices $n \neq n'$ have vanishing solutions since there is no inhomogeneous term. Surprisingly, these equations show a decoupling of partial waves. s–wave scattering only influences the s–wave coefficient of the T–matrix and similarly for d–wave coefficients.

The solutions to the equations 13.17 are readily obtained. For example, I write $\hat{T}^e_{1,1} = t^e_o\tau_o + t^e_1\tau_1$ (the other τ's are not involved). This leads to two equations for t^e_o and t^e_1 which I write as

$$\begin{pmatrix} t^e_o \\ t^e_1 \end{pmatrix} = \begin{pmatrix} 0 \\ \delta_d \end{pmatrix} + \delta_d \begin{pmatrix} g_2 & g_o \\ g_o & g_2 \end{pmatrix} \begin{pmatrix} t^e_o \\ t^e_1 \end{pmatrix} \tag{13.18}$$

After a bit of linear algebra I find

$$\begin{pmatrix} t^e_o \\ t^e_1 \end{pmatrix} = \frac{1}{det} \begin{pmatrix} 1 - \delta_d g_2 & \delta_d g_o \\ \delta_d g_o & 1 - \delta_d g_2 \end{pmatrix} \begin{pmatrix} 0 \\ \delta_d \end{pmatrix} \tag{13.19}$$

with $det = (1 - \delta_d g_2)^2 - (\delta_d g_o)^2$. Finally, this leads to

$$\hat{T}^e_{1,1} = \frac{\delta_d^2 g_o \tau_o + \delta_d(1 - \delta_d g_2)\tau_1}{(1 - \delta_d g_2)^2 - (\delta_d g_o)^2}. \tag{13.20}$$

Similarly, I find

$$\hat{T}^o_{1,1} = \frac{\delta_d^2 g_o \tau_o - \delta_d(1 - \delta_d g_2)\tau_1}{(1 - \delta_d g_2)^2 - (\delta_d g_o)^2}. \tag{13.21}$$

At $q = 0$, $\phi_p = \phi_{p'} = \phi_k$ and the T-matrix becomes

$$\hat{T}_{\phi_k}(\omega) = \hat{T}_o(\omega) + \hat{T}_1^-(\omega)\cos 2\phi_k + \hat{T}_1^+(\omega) \tag{13.22}$$

with

$$\hat{T}_o(\omega) = \frac{(U_o^2 + \delta_s^2) g_o \tau_o + U_o \tau_3 + \delta_s \tau_1}{1 - (U_o^2 + \delta_s^2) g_o^2}, \tag{13.23}$$

$$\hat{T}_1^-(\omega) = \left(\frac{1 - \delta_d g_2}{(1 - \delta_d g_2)^2 - (\delta_d g_o)^2} \right) \delta_d \tau_1, \tag{13.24}$$

$$\hat{T}_1^+(\omega) = \left(\frac{\delta_d^2 g_o}{(1 - \delta_d g_2)^2 - (\delta_d g_o)^2} \right) \tau_o. \tag{13.25}$$

The T–matrix has now an explicitly k–dependent and off–diagonal term . Also observe, that there is actually a contribution $(\hat{T}_1^+(\omega))$ to the k–independent, diagonal part involving the new scattering parameter δ_d. Both new contributions have an impact on the impurity averaged self energy $\hat{\Sigma}$, (see next chapter).

13.3 Constitutive Equation for the Order Parameter Scattering Strength

For simplicity, let me consider $\delta_s = 0$ first, that is, I consider a d–wave SC without any (not even a repulsive) s–wave component in the pairing potential V. This is probably unrealistic, however, recent numerical work [89] has shown that the induced (extended) s–wave order parameter has a vanishing $q = 0$–component due to sign changes on the lattice diagonals, and is thus not relevant for this discussion.

As before, I insert the new T–matrix into Eq. 12.5 and separate terms. I find

$$\delta_d \left(\frac{1}{N_o V} + T \sum_\omega \frac{(1-\delta_d g_2)}{(1-\delta_d g_2)^2 - (\delta_d g_o)^2} \langle 2\cos^2(2\phi) \int d\xi \frac{\Delta_\phi^2 - \omega^2 - \xi^2}{(\omega^2+\xi^2+\Delta_\phi^2)^2} \rangle_\phi \right)$$
$$= -T \sum_\omega [\frac{U_o^2 g_o}{1-(U_o g_o)^2} + \frac{\delta_d^2 g_o}{(1-\delta_d g_2)^2 - (\delta_d g_o)^2}] \langle \int d\xi \frac{2\Delta\cos^2(2\phi)\, i\omega}{(\omega^2+\xi^2+\Delta_\phi^2)^2} \rangle_\phi \quad (13.26)$$

where $\langle \ldots \rangle_\phi$ stands for the angular integral $\int \frac{d\phi}{2\pi} \ldots$. After integration over the energy ξ I eliminate the $1/(N_o V)$–term by use of the gap equation 10.6 and obtain (after canceling an overall constant 2π)

$$\delta_d\ T\ \textstyle\sum_\omega\ \langle \cos^2(2\phi) \left(\frac{1-\delta_d g_2}{(1-\delta_d g_2)^2 - (\delta_d g_o)^2} \frac{\Delta_\phi^2}{(\omega^2+\Delta_\phi^2)^{3/2}} \right.$$
$$\left. - \frac{\delta_d g_2 - (\delta_d g_2)^2 + (\delta_d g_o)^2}{(1-\delta_d g_2)^2 - (\delta_d g_o)^2} \frac{1}{(\omega^2+\Delta_\phi^2)^{1/2}} \right) \rangle_\phi$$
$$= -T \textstyle\sum_\omega\ [\frac{U_o^2 g_o}{1-(U_o g_o)^2} + \frac{\delta_d^2 g_o}{(1-\delta_d g_2)^2 - (\delta_d g_o)^2}] \langle \frac{\Delta\cos^2(2\phi)\, i\omega}{(\omega^2+\Delta_\phi^2)^{3/2}} \rangle_\phi \quad (13.27)$$

This lengthy expression reduces properly to Eq. 12.11 if I expand the denominators and consider terms up to first order in δ_d. However, due to δ_d in the denominators Eq. 13.27 will prevent δ_d from diverging. Because of its nonlinearity, the solutions of this constitutive equation are only numerically accessible. I will show the results in the next chapter.

I am ending this chapter by again pointing out the approximations used to obtain the new T–matrix and the constitutive equation 13.27.

- I assume short ranged order parameter perturbations that are characterized by their volume integral $\delta\Delta_k(q=0)$.

- I consider a q–independent form of the order parameter perturbations with a k–dependence motivated by the bulk order parameter.

- All the calculations are based on the weak–coupling BCS–theory.

I then choose a pairing potential that limits the number of partial waves contributing to scattering. This is not a new approximation, rather a specification to the case of interest. After obtaining the T–matrix I then use the gap equation to write a constitutive equation for the special case of a pure d–wave pairing potential V. The constitutive equation allows the determination of the only parameter left in the theory, the magnitude of order parameter perturbations δ_d. Therefore, δ_d is not a free parameter but is determined by the requirement of self–consistency of the BCS–theory.

CHAPTER 14
ORDER PARAMETER PERTURBATIONS AND SELF ENERGIES

14.1 The Order Parameter Scattering Strength

The constitutive equation 13.27 allows me to self–consistently determine the magnitude of the order parameter perturbations δ_d. In contrast to the first order result Eq. 12.11, δ_d from Eq. 13.27 is not just a function of T/T_c and U_o but depends explicitly on the cut–off frequency ω_o and the coupling V. I choose for the normal density of states $N_o = 0.01$, $\omega_o = 30$ and $V = 28.3108$, so that $T_c = 1$. Therefore, all energies (frequencies, temperatures) are in units of T_c ($\hbar = k_B = 1$). With $N_oV = 0.283108$ I am at the limit of what is considered "weak–coupling". Since $N_o \sim 1/E_F$, $E_F/T_c \sim 100$, appropriate for the High–T_c SC's. Recall that the maximum of the bulk order parameter at $T = 0$ is given by $\Delta/T_c = 2.14$ for a 2D $d_{x^2-y^2}$ SC with cylindrical Fermi surface.

I first show the dependence of δ_d as a function of the impurity scattering strength U_o at a low temperature $T/T_c = 0.01$, see Fig. 14.1. Both the first order and the fully self–consistent (involving all orders) results rise monotonically and saturate as one approaches the unitary limit $N_o\pi U_o \gg 1$. A peculiar feature is that the all order result is actually slightly higher than the first order result in the Born–limit $N_o\pi U_o \ll 1$. For large U_o, however, the first order result is higher. This I expected from the fact that, for $\delta_d N_o \pi \sim 1$, the denominators in

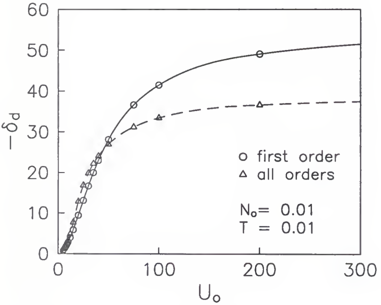

Figure 14.1: Order parameter scattering strength vs. normal scattering strength. At $T = 0.01T_c$ both the first order and all order result for $-\delta_d$ rise monotonically and saturate in the unitary scattering limit, $N_o\pi U_o \gg 1$. The saturated value for the all order result is about $-\delta_d N_o \pi \sim 1.2$, with $N_o = 0.01$ in units of inverse T_c.

Eq. 13.27 reduce the magnitude of δ_d compared to the first order result. The all order result saturates at about $-\delta_d N_o \pi \sim 1.2$. The zeroth order result (from Eq. 12.5 with the standard T–matrix) is about an order of magnitude smaller at this temperatures.

Next, I look at the temperature dependence of the order parameter scattering strength, Fig.14.2. For low temperatures, there is only a weak T–dependence.

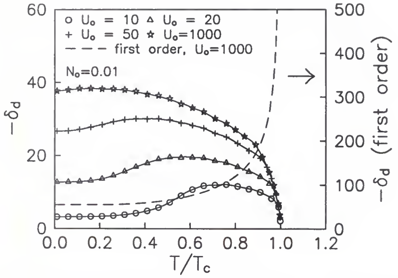

Figure 14.2: Order parameter scattering strength vs. temperature. For low temperature there is only a weak T–dependence. Close to T_c, the first order result (dashed line) diverges like $(1-T/T_c)^{-1/2}$ whereas the all order result vanishes with the bulk order parameter Δ like $(1-T/T_c)^{1/2}$. Observe that the maximum of the all order curves moves to lower temperatures as U_o increases. For $U_o \to \infty$, the maximum approaches $T = 0$, and the temperature dependence of $-\delta_d$ resembles that of the bulk order parameter Δ.

The all order data show a maximum that moves to lower temperatures as U_o increases. For $U_o \to \infty$, the maximum value is probably (within numerical uncertainty) located at $T = 0$. Therefore, the temperature dependence of $-\delta_d$ strongly resembles that of the bulk order parameter Δ. As advertised, the behavior of the first order result is strikingly different, especially at temperatures close to T_c

where it diverges like $(1-T/T_c)^{-1/2}$. The all order data vanish at T_c with the bulk order parameter Δ like $(1-T/T_c)^{1/2}$. Although my local approximation for the order parameter perturbations can be only justified for temperatures for which the Ginzburg-Landau coherence length $\xi_T = \xi_{T=0}/(1-T/T_c)^{1/2}$ is less than the average inter–impurity distance, for the small $\xi_{T=0}$ of the high–T_c SC's and low impurity concentrations, the temperature at which the approximation fails can be as high as $0.99\,T_c$. Therefore, my approximation is justified for the systems of interest at all temperatures but the very small GL-regime.

14.2 T–matrix and the Disorder Averaged Self Energy

Having obtained the order parameter scattering strength δ_d, I now make use of the SCTMA (see chapter 10) to compute the disorder averaged self–energy $\hat{\Sigma}$. Eq. 10.15 is a self–consistency equation for the diagonal ($\propto \tau_o$) and off–diagonal ($\propto \tau_1$) components of $\hat{\Sigma}$, since the g_o and g_2 of the T–matrix 13.22 are depending on the self–energy via the disorder–averaged Green function

$$\hat{G}(k,\omega) = (i\omega - \xi\tau_3 - \Delta_\phi\tau_1 - \hat{\Sigma}_\phi)^{-1}\,. \tag{14.1}$$

The self–consistency equation 10.15 must be solved numerically. I show the results below.

For better comparison with standard notation (e.g. Ref. [59]), I rescale the scattering strengths and the functions g_o and g_2. Introducing

$$c = \frac{1}{U_o N_o \pi} \quad c_f = \frac{1}{\delta_d N_o \pi}\,, \tag{14.2}$$

$G_o = g_o/(N_o\pi)$ and $G_2 = g_2/(N_o\pi)$ and $\Gamma = n_i/(N_o\pi)$ (the scattering rate in the normal state, i. e., for $T > T_c$) the self–consistency equation for the considered case reads

$$\hat{\Sigma}_\phi = \Gamma\frac{G_o\tau_o - c\tau_3}{c^2 - G_o^2} + \Gamma\frac{G_o\tau_o}{(c_f - G_2)^2 - G_o^2} + \Gamma\frac{(c_f - G_2)\tau_1}{(c_f - G_2)^2 - G_o^2}\cos 2\phi. \tag{14.3}$$

For a particle–hole symmetric system, the τ_3–component of the self–energy is vanishing [93], so only τ_o– and τ_1–components (Σ_o and Σ_1, correspondingly) need to be determined. For real frequencies ω, these self–energy components are complex functions of ω. In the standard case without order parameter scattering, only Σ_o is nonvanishing (as can be seen from above by setting $\delta_d = 0$). Then one can relate the imaginary part of the self energy to a scattering rate or the relaxation time (e.g. see [59]). In the case here, however, I also have a τ_1–component Σ_1 of the self energy which also has an imaginary part. The concept of a scattering rate (on this microscopic level) becomes now questionable. What should one think of a scattering rate that is a matrix in particle–hole space? Unfortunately, I have to abandon this intuitive concept for now, until other methods (like a Boltzmann equation approach) might show what the equivalent of the standard scattering time is for a system with order parameter scattering.

In terms of the dimensionless parameter c one distinguishes three regimes of scattering strengths. $c >> 1$ corresponds to the Born limit of weak scattering, $c \to 0$ is the strong scattering regime, and $c \sim 1$ is the intermediate scattering regime. It is instructive to replot Fig. 14.1 as a graph for c_f vs. c, see Fig. 14.3. The plot reveals several features:

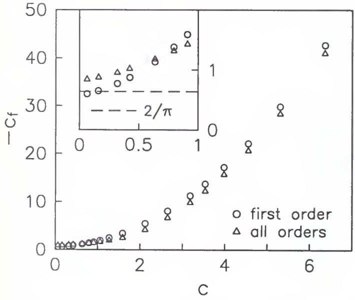

Figure 14.3: Dimensionless order parameter scattering strength vs. dimensionless normal scattering strength. In the Born limit, $c \gg 1$, $-c_f \gg c$, so that order parameter scattering is probably unimportant. However, in the intermediate scattering regime, $c \sim 1$, $-c_f \sim c$, so both scattering processes are important. In the strong scattering regime, $c \to 0$, $-c_f$ remains finite, but can be close to $2/\pi$ (see inset), which allows the new self energy contributions to be large, see text for more detailed discussion.

- In the Born limit ($c \gg 1$), $-c_f \gg c$. Therefore, order parameter scattering is probably unimportant, since the denominators of the new contributions to the self energy Eq. 14.3 are much larger than that of the standard term.
- In the intermediate scattering regime ($c \sim 1$), $-c_f \sim c$, and by the same reasoning as above all contributions to the self energy are important.
- In the strong scattering regime ($c \to 0$), $-c_f$ remains finite. However, be-

cause of the different structure of the denominators of the new contributions in Eq. 14.3, this does not immediately render the new terms unimportant compared to the standard term. For a pure d-wave SC $G_2(\omega = 0) = -2/\pi$, so that even for $-c_f \sim 1/1.2$, $(c_f - G_2(\omega = 0)) \sim 0.2$. This illustrates, that the denominator structure enhances the effect of the order parameter scattering, though its bare strength is less than that of the standard scattering term.

I am primarily interested in the last (strong scattering) regime, since the standard approach has been successful in explaining the power laws of thermodynamic quantities like the London penetration depth observed in the high-T_c SC's. The above argument stresses the necessity of a numerical, quantitative evaluation of the self energy components, since there are too many energy scales in the system to isolate a frequency regime in which power law expansions of the self energy are valid.

14.3 Diagonal Self Energy Component Σ_0 and the Density of States

For unitary scattering, i.e. $c = 0$, in Fig. 14.4 I show the imaginary part of the diagonal self energy Σ_o ($\hat{\Sigma} = \Sigma_o \tau_o + \Sigma_1 \tau_1 \cos 2\phi$). For illustration purposes,

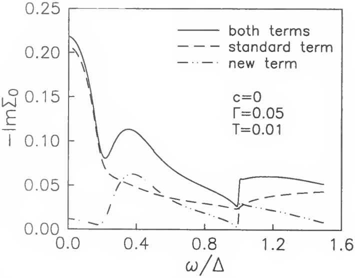

Figure 14.4: Imaginary part of the diagonal self energy component Σ_o vs. frequency. For unitary scattering ($c = 0$) the standard term (dashed line) shows a peak at zero frequency and a characteristic $1/\omega$–decay above an energy scale $\gamma \sim \sqrt{\Gamma\Delta}$. The new term has a wide peak at intermediate frequencies, but is small at lower frequencies. As a result, the DOS and the resulting thermodynamic properties have minor changes at intermediate temperatures, $T \sim 0.5T_c$.

I choose a rather large normal state scattering rate $\Gamma = 0.05$. The standard term (dashed line) has a zero frequency peak and a characteristic $1/\omega$–decay above $\gamma \sim \sqrt{\Gamma\Delta}$. γ is roughly the energy scale below which the self–consistency aspect of Eq. 10.15 becomes important in the standard theory without order parameter scattering. The new term has a wide peak at intermediate frequencies, but is small at lower frequencies. $-Im\Sigma_o$ is the main ingredient in the determination

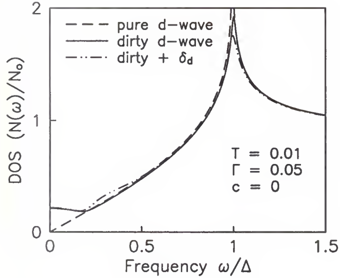

Figure 14.5: Quasiparticle density of states (DOS) vs. frequency. The pure d–wave SC shows linear dependence at low frequencies, the standard theory (unitary scattering, $c = 0$) of a dirty d–wave SC gives a basically flat DOS for frequencies below $\gamma \sim \sqrt{\Gamma\Delta}$. This translates in linear (pure d–wave) and quadratic (dirty d–wave) behavior for the London penetration depth, in agreement with experiments on clean and dirty samples. The new scattering due to δ_d leads only to a mild hump at intermediate frequencies, even for the rather large value of $\Gamma = 0.05$ (corresponding to a very impure sample). Therefore, the new scattering has no qualitative bearing on thermodynamic properties.

of the quasiparticle DOS, see Eqs. 10.7 and 14.1. Since the low energy behavior of $-Im\Sigma_o$ is essentially unchanged, so are the low energy DOS and the resulting thermodynamic quantities. I show the new DOS together with the standard result and the DOS of a pure d–wave SC in Fig. 14.5. The new term affects the DOS only at intermediate frequencies and the thermodynamics only mildly at intermediate temperatures, $T \sim 0.5T_c$. Not just for the sake of completeness,

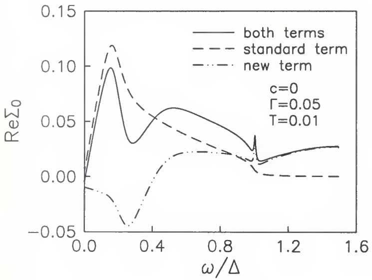

Figure 14.6: Real part of the diagonal self energy component Σ_o vs. frequency. $Re\Sigma_o$ is proportional to ω at frequencies below $\gamma \sim \sqrt{\Gamma\Delta}$. The new term again adds a hump at intermediate frequencies. $Re\Sigma_o$ has usually only minor impact on physical observables.

I also show the real part of Σ_o in Fig. 14.6. $Re\Sigma_o$ has usually small impact on physical quantities. It is important, though, that at frequencies below γ it rises linearly from zero, as it does without order parameter scattering. Again, the new term adds a hump at intermediate frequencies.

14.4 Results for the Off–Diagonal Self Energy Component Σ_1

The off–diagonal self energy component Σ_1 is an entirely new term, so I can not compare to the standard theory here. Instead, in Fig. 14.7 I show its frequency

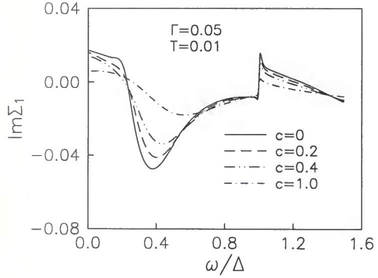

Figure 14.7: Imaginary part of the off–diagonal self energy component Σ_1 vs. frequency. $Im\Sigma_1$ is finite and positive below an c−−(δ_d)–dependent energy scale. With increasing c (decreasing $-\delta_d$) $Im\Sigma_1$ becomes smaller in overall magnitude.

dependence for various scattering strengths c. The most important aspect of the curves is the fact that $Im\Sigma_1$ is finite and positive below a new energy scale that in the strong scattering regime depends only weakly on c (or more accurate, on δ_d). Observe, that the crossover to positive values of $Im\Sigma_1$ stays almost the same for $c < 1$, and only slowly moves to larger frequencies as c increases (and $-\delta_d$ decreases). The crossover frequency does not depend on γ in any simple fashion, and for the reasonable values of the normal scattering rate the crossover frequency is larger than γ. On general symmetry grounds $Im\Sigma_1$ must be antisymmetric about the Fermi level. The surprise is that rather than going through zero,

$Im\Sigma_1$ has a finite step at the Fermi level. This feature, in conjunction with the linear behavior of $Re\Sigma_o$, makes the new self energy component important when it comes to transport properties, as will be shown in the next chapter.

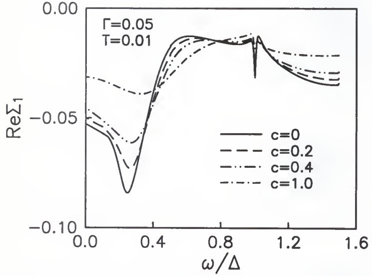

Figure 14.8: Real part of the off–diagonal self energy component Σ_1 vs. frequency. $Re\Sigma_1$ is finite and negative at all frequencies below the bulk order parameter Δ. It is a frequency dependent renormalization of the bulk order parameter. However, since it is always much smaller than Δ itself, it is of negligible importance.

The real part of the off–diagonal self energy component Σ_1 is of minor importance when it comes to physical observables. It is instructive to realize, that it is $Re\Sigma_1$, rather than δ_d, that renormalizes the bulk order parameter Δ. $Re\Sigma_1$ is negative for all frequencies, and therefore it is a frequency dependent reduction of the bulk order parameter. However, it is much smaller in magnitude than the

bulk order parameter Δ_k. Since it enters equations always in addition to Δ it has negligible effects. This justifies partially our use of BCS rather than Eliashberg theory, since large frequency dependent corrections to Δ_k would necessitate the use of the strong coupling Eliashberg theory.

CHAPTER 15
APPLICATION: MICROWAVE CONDUCTIVITY

As an example of the effect of the order parameter scattering on transport properties I will discuss the "microwave" conductivity of a d–wave SC. It is nothing but the conductivity in the case of a extreme Type II SC (like the high–T_c SC's) where the penetration depth is much larger than the coherence length. It then suffices to consider wave vectors q of the current response that are approximately zero. The microwave conductivity $\sigma(T,\Omega)$ (Ω being the microwave frequency) is in general a tensor that within linear response is determined by the retarded current–current correlation function (Kubo formula). A detailed discussion of the formalism can be found in Refs. [59, 94]. I just quote the result for the diagonal components of the conductivity tensor.

$$\sigma(T,\Omega) = \frac{ne^2}{2m\Omega}\int_{-\infty}^{\infty} d\omega\,[\tanh(\beta\omega/2) - \tanh(\beta(\omega-\Omega)/2)]\,S(\omega,\Omega,T), \qquad (15.1)$$

where n is the electron density, e and m the electron charge and mass, respectively, and

$$S(\omega,\Omega,T) = -\tfrac{1}{2}\mathrm{Im}\int_0^{2\pi}\tfrac{d\phi}{2\pi}\left(\frac{\tilde\omega'_+(\tilde\omega_+ + \tilde\omega'_+) + \tilde\Delta'_{\phi+}(\tilde\Delta_{\phi+} - \tilde\Delta'_{\phi+})}{(\xi_+ + \xi'_+)\xi'_+\xi_+} + \frac{\tilde\omega'_-(\tilde\omega_+ + \tilde\omega'_-) + \tilde\Delta'_{\phi-}(\tilde\Delta_{\phi+} - \tilde\Delta'_{\phi-})}{(\xi_+ - \xi'_-)\xi'_-\xi_+}\right). \qquad (15.2)$$

Here, $\tilde{\omega}_\pm = \tilde{\omega}(\omega \pm i0^+)$ with $\tilde{\omega} = \omega - \Sigma_o(\omega)$, $\tilde{\Delta}_{\phi,\pm} = \tilde{\Delta}_\phi(\Delta_\phi \pm i0^+)$ with $\tilde{\Delta}_\phi = \Delta_\phi + \Sigma_1(\omega)\cos 2\phi$, and $\xi_\pm = \mathrm{sgn}(\omega)\sqrt{\tilde{\omega}_\pm^2 - \tilde{\Delta}_{\phi,\pm}^2}$. The infinitesimal $\pm i0^+$ indicates whether one has to evaluate the self energies above or below the branch cut in the complex ω–plane. The primes indicate that the corresponding quantities are to be evaluated at $\omega - \Omega$.

In the limit of vanishing microwave frequency $\Omega \to 0$ the expressions can be somewhat simplified. For $T \gg \Omega$, $[\tanh(\beta\omega/2) - \tanh(\beta(\omega-\Omega)/2)]/2\Omega \to -\partial \mathrm{F}(\omega)/\partial\omega$ with $\mathrm{F}(\omega)$ the Fermi function. The first term in the integrand of $S(\omega, \Omega, T)$ becomes simply $\tilde{\omega}_+^2/\xi_+^3$. This term, however, turns out to give only a very small contribution at any experimentally accessible temperature. Nevertheless, it has theoretical significance, since at $T = 0$ it gives a nonzero contribution to the conductivity that is *independent* of the impurity concentration, $\sigma_o = ne^2/(m\pi\Delta)$, as first pointed out by Lee [95]. The second term in the integrand of Eq. 15.2 remains complicated, but it is instructive to write it partly in terms of the real and imaginary parts of the self energies. Multiplying numerator and denominator with $(\xi_+ + \xi_-)$ I obtain (ignoring an overall factor)

$$\frac{(\omega - Re\Sigma_o)\tilde{\omega}_- - Im\Sigma_1 \cos 2\phi \tilde{\Delta}_{\phi+}}{-Im\Sigma_o(\omega - Re\Sigma_o) - Im\Sigma_1(\Delta + Re\Sigma_1)\cos^2(2\phi)} \frac{Re\xi_+}{\xi_+\xi_-} \tag{15.3}$$

For small frequencies I showed in the previous chapter that $Im\Sigma_o$ is finite and negative, $Re\Sigma_o$ vanishes linearly with ω, however $Im\Sigma_1$ is nonzero and positive. This implies that the first fraction of 15.3 has a pole at a certain angle ϕ_o. This pole, however, is countered by a zero in $Re\xi_+$. Together, the term 15.3 has a cusp at the angle ϕ_o for small frequencies. Such features do not exist in the standard

theory with no Σ_1 present. Thus, this analysis hints to the importance of the new off–diagonal self energy Σ_1.

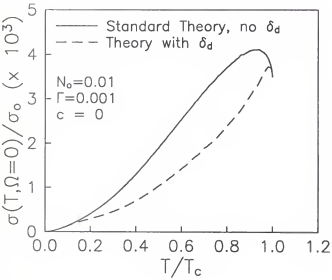

Figure 15.1: Microwave conductivity vs. temperature. For the normal state scattering strength $\Gamma = 0.001$ I show the $\sigma(T, \Omega = 0)$ for the new theory including order parameter scattering and the standard theory, both in the unitary scattering limit $c = 0$. At very low temperatures the curves are almost identical. Above $T \sim 0.1T_c$ the new theory gives a much lower conductivity due to the hump in $Im\Sigma_o$. The graph is roughly linear until it reaches a maximum just below T_c. At T_c the conductivity is given by $\sigma(T_c) = \frac{ne^2}{m}\frac{1}{2\Gamma}$. The standard theory has a much broader 'coherence' peak until it also reaches the normal state conductivity $\sigma(T_c)$.

In Fig. 15.1 I show the zero–frequency microwave conductivity $\sigma(T, \Omega = 0)$ for the new theory including order parameter scattering compared to the standard theory without order parameter scattering. At very low temperatures the curves are almost identical and behave like T^2. Above $T \sim 0.1T_c$ the new the-

ory has much lower conductivity due to the hump in $Im\Sigma_o$ which leads to an increased scattering rate compared to the standard theory without order parameter scattering. The graph of the new theory is roughly linear until it reaches a maximum just below T_c. At T_c the conductivity should be given by the normal state conductivity, $\sigma(T_c) = \frac{ne^2}{m}\frac{1}{2\Gamma}$. The new theory fulfills this requirement due to the vanishing of δ_d at T_c. The standard theory has a much broader peak (due to the 'coherence factors' in the language of BCS–theory). It rises much faster at intermediate temperatures and reaches the normal state conductivity $\sigma(T_c)$, too.

In Fig. 15.2 I show the low temperature part of Fig. 15.1. As mentioned above, below $T \sim 0.1T_c$ there are only small differences between the new theory including order parameter scattering and the standard theory. The new theory has a slightly enhanced conductivity above $T \sim \gamma \sim \sqrt{\Gamma\Delta}$ which can be traced to the new self energy contribution Σ_1. This enhancement leads to approximately linear T–dependence above $T \sim \gamma$. However, below that temperature the conductivity behaves like T^2 as it did in the standard theory without order parameter scattering. Above $T \sim 0.1T_c$ the hump in $Im\Sigma_o$ leads to a suppression of the conductivity due to the increased scattering. The overall shape of the conductivity of the new theory appears linear after the initial quadratic rise. In contrast, the standard theory is essentially quadratic over the total temperature range of the graph.

I mentioned in the previous chapter that the order parameter scattering might also be of importance in the case of intermediate normal scattering strength. For $c = 0.3$ (which corresponds to U_o of about the Fermi energy) I show again

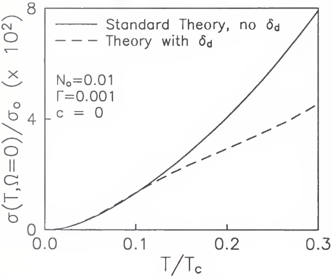

Figure 15.2: Microwave conductivity vs. temperature at low temperatures. For the normal state scattering strength $\Gamma = 0.001$ and in the unitary scattering limit $c = 0$ the new theory including order parameter scattering and the standard theory show only small differences below $T \sim 0.1T_c$. The new theory gives slightly enhanced conductivity but still behaves like T^2 at very low temperatures $T < \gamma$. Above $T \sim 0.1T_c$ the new theory gives a much lower conductivity due to the hump in $Im\Sigma_o$. The graph of the new theory appears linear for $T > \gamma$. The standard theory behaves like T^2 for the total temperature range in this graph.

the zero–frequency microwave conductivity for both the standard and the new theory. As before there is an enhancement at low temperatures and suppression of the conductivity at higher temperatures. The low–T enhancement is much more visible than in the unitary scattering case. However, the major difference between the curves is still at intermediate temperatures. The large residual conductivity at low T is in strong contrast to experiments on clean high–T_c samples. Therefore,

this case is of pure theoretical interest for the time being, lacking an experimental realization at the moment.

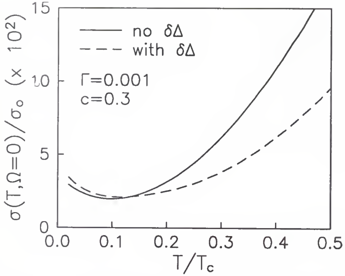

Figure 15.3: Microwave conductivity vs. temperature for nonunitary normal scattering. For $\Gamma = 0.001$ I show the $\sigma(T, \Omega = 0)$ for the new theory and the standard theory, for an intermediate scattering strength, $c = 0.3$. At low temperatures the new theory gives a slightly higher conductivity. However, the major deviation is at higher temperatures, where the conductivity is suppressed due to the additional hump in $Im\Sigma_o$.

So far, I have only considered the case of vanishing microwave frequency, $\Omega = 0$. In the standard theory finite Ω lower the conductivity, but do not change the low temperature power law. I do not expect this to be different in the theory including order parameter scattering. Inelastic scattering, e.g. due to spin fluctuations, is negligible at low temperatures but rises approximately like $(T/T_c)^3$,

and it therefore becomes important at intermediate temperatures (depending on Γ). Beyond such a crossover temperature inelastic scattering dominates, hence the conductivity will decrease. The increase at low T due to impurity scattering and the decrease at higher T due to inelastic scattering give rise to the peak in the conductivity seen in experiments. This peak is thus not related to the 'coherence' peak shown in Fig. 15.1. I have performed preliminary calculations on the conductivity including finite frequencies and inelastic scattering. However, because of their preliminary nature I refrain from including these results in this thesis.

CHAPTER 16
CONCLUSIONS TO PART II

I have investigated the effect of nonmagnetic impurities on a d–wave SC. In addition to the standard potential scattering, I included the scattering due to local perturbations of the order parameter around the impurity site. Since these perturbations are not a priori small, I determined them self–consistently via the gap equation. To do that, I employed a local approximation in which I replaced the short ranged spatial dependence of the perturbations by a Dirac δ–function. I was able to analytically compute the momentum dependent T–matrix of a single impurity in a bulk d–wave SC. I analyzed the validity of the standard self–consistent T–matrix approximation (SCTMA) for the case of a 2D d-wave SC, and concluded that the SCTMA is qualitatively sufficient to describe the effects of dilute concentrations of impurities on such systems. I numerically determined the disorder averaged self energy $\hat{\Sigma}$ of the bulk system employing the SCTMA.

Two new contributions show up as a consequence of the new scattering mechanism, one modifying the diagonal self energy Σ_o, the other one a completely new off–diagonal term Σ_1 with the same angle dependence as the bulk order parameter. The new self energy contributions have negligible effect on thermodynamic properties, since they add only a minor feature to the density of states away from the Fermi level. Their impact on transport properties is more significant. At low temperatures the off–diagonal contribution Σ_1 slightly enhances the

microwave conductivity (at zero frequency), making it appear linear for temperatures $T > \gamma \sim \sqrt{\Gamma\Delta}$. However, this effect is small, and the very low temperature behavior $\sim T^2$ is unchanged. At higher temperatures the second contribution has a more obvious impact, since it reduces the conductivity significantly in comparison to the standard theory without order parameter scattering. However, because of the dramatic increase of inelastic scattering at higher temperatures (not considered this far) this suppression of the conductivity will be experimentally obscured due to the much stronger suppression as a consequence of inelastic scattering.

It is thus questionable, whether experiments of the current resolution will be able to detect the effects of order parameter scattering on transport properties. In the real high–T_c materials there might also be other scattering mechanisms due to other impurities than considered. From the theorists point of view, the new theory can not explain the linear temperature dependence at very low T, though it provides a step in the right direction. Open questions concern the dependence of the conductivity on the external frequency Ω and the influence of inelastic scattering.

These issues, however, will be addressed at a later time and not within the framework of this thesis. For the time being I will rest my case.

CHAPTER 17
FINAL CONCLUSIONS

I considered two systems with small amounts of impurities added to an otherwise pure material. In the first part I studied the conductance and susceptibility of clean metal point contacts and metal–insulator–metal tunnel junctions in the presence of impurities with two states of degenerate energy. Depending on the kind of interaction of the impurity with the conduction electrons, the low temperature behavior of the physical properties was qualitatively changed, compared to a system with standard potential scattering. I have studied the nonequilibrium aspects of these systems in the case of a static bias V. Scaling of the nonlinear conductance was observed at low temperatures as well as deviations from scaling at higher temperatures.

In the second part I studied the influence of standard, nonmagnetic impurities on a d–wave superconductor. The nodes of the order parameter of the d–wave SC lead to qualitative different behavior for both thermodynamical and transport properties when compared to the metallic, s–wave SC's. I included the response of the order parameter to the impurity potential as an additional scattering mechanism. Though important at intermediate temperatures, the low temperature behavior of the microwave conductivity was unchanged when compared to standard theories.

In conclusion, the first system showed dramatic qualitative changes of observ-

ables upon addition of small amounts of impurities. Such changes are present also in the second system, however, my modification of the standard treatment turned out to be a quantitative effect, leaving the qualitative behavior unaffected.

BIBLIOGRAPHY

[1] D. C. Ralph and R. A. Buhrman, Phys. Rev. Lett. **69**, 2118 (1992).

[2] J. G. Bednorz and K. A. Müller, Z. Phys. **B64**, 189 (1986).

[3] H. K. Onnes, Comm. Leiden **120b**, (1911).

[4] P. W. Anderson, Phys. Rev. **124**, 41 (1961).

[5] C. Zener, Phys. Rev. **81**, 440 (1951).

[6] J. R. Schrieffer and P. A. Wolff, Phys. Rev. **B149**, 491 (1966).

[7] K. Ingersent, preprint (1996).

[8] J. Kondo, Prog. Theoret. Phys. **32**, 37 (1964).

[9] Y. Kuramoto, Z. Phys. **B53**, 37 (1983).

[10] P. Coleman, Phys. Rev. **B29**, 3035 (1984).

[11] E. Müller–Hartmann, Z. Phys. **B57**, 281 (1984).

[12] N. E. Bickers, Rev. Mod. Phys. **59**, 845 (1987).

[13] P. Nozières and A. Blandin, J. Phys. (Paris) **41**, 193 (1980).

[14] D. C. Ralph, J. von Delft, A. A. W. Ludwig and R. A. Buhrman, Phys. Rev. Lett. **72**, 1064 (1994).

[15] K. G. Wilson, Rev. Mod. Phys. **47**, 773 (1975).

[16] H. R. Krishna-murthy, J. W. Wilkins and K. G. Wilson, Phys. Rev. **B21**, 1003, 1044 (1980).

[17] N. Andrei, Phys. Rev. Lett. **45**, 379 (1980).

[18] N. Andrei, K. Furuya and J. H. Lowenstein, Rev. Mod. Phys. **55**, 331 (1983).

[19] P. B. Wiegmann, J. Phys. **C14**, 1463, (1981).

[20] A. M. Tsvelick and P. B. Wiegmann, Adv. Phys. **32**,453 (1983).

[21] N. Kawakami and A. Okiji, Phys. Lett. **A86**, 483 (1981).

[22] A. Okiji and N. Kawakami, J. Appl. Phys. **55**, 453 (1985).

[23] A. A. Abrikosov, Physics **2**, 5, 61 (1965).

[24] P. W. Anderson and G. Yuval, Phys. Rev. Lett. **23**, 89 (1969).

[25] P. Nozières, J. Low Temp. Phys. **17**, 31 (1974).

[26] A. A. W. Ludwig and I. Affleck, Phys. Rev. Lett. **67**, 3160 (1991).

[27] I. Affleck and A. A. W. Ludwig, Phys. Rev. **B48**, 7297 (1993).

[28] F. D. M. Haldane, J. Phys. **C14**, 2585 (1991).

[29] V. J. Emery and S. Kivelson, Phys. Rev. **B46**, 10812 (1992); Phys. Rev. Lett. **71**, 3701 (1993).

[30] D.L. Cox, Phys. Rev. Lett. **59**, 1240 (1987); Physica (Amsterdam) **153–155C**, 1642 (1987); J. Magn. Magn. **76&77**, 53 (1988).

[31] C. L. Seaman, M. B. Maple, B. W. Lee, S. Ghamaty, M. S. Torikachvili, J.-S. Kang, L. Z. Liu, J. W. Allen and D. L. Cox, Phys. Rev. Lett. **67**, 2882 (1991).

[32] B. Andraka and A.M. Tsvelik, Phys. Rev. Lett. **67**, 2886 (1991).

[33] A. Zawadowski, Phys. Rev. Lett. **45**, 211 (1980).

[34] K. Vladar and A. Zawadowski, Phys. Rev. **B28**, 1564, 1582, 1596 (1983).

[35] A. Muramatsu and F. Guinea, Phys. Rev. Lett. **57**, 2337 (1986).

[36] S. Katayama, S. Maekawa and H. Fukuyama, J. Phys. Soc. Jpn. **56**, 697 (1987).

[37] T. Ishiguro, H. Kaneko, Y. Nogami, H. Ishimoto, H. Nishiyama, J. Tsukamoto, A. Takahashi, M. Yamaura, T. Hagiwara and K. Sato, Phys. Rev. Lett. **69**, 660 (1992).

[38] J. Appelbaum, Phys. Rev. Lett. **17**, 91 (1966).

[39] P. W. Anderson, Phys. Rev. Lett. **17**, 95 (1966).

[40] M. H. Hettler, J. Kroha and S. Hershfield, preprint (1996).

[41] S. E. Barnes, J. Phys. **F6**, 1375 (1976); **F7**, 2637 (1977).

[42] T. A. Costi, P. Schmitteckert, J. Kroha and P. Wölfle, Phys. Rev. Lett. **73**, 1275 (1994).

[43] D. L. Cox and A. E. Ruckenstein, Phys. Rev. Lett. **71**, 1613 (1993).

[44] J. Kroha, Ph. D. Thesis, Universität Karlsruhe (1993).

[45] D. C. Langreth, 1975 NATO Advanced Study Institute on Linear and Nonlinear Electron Transport in Solids, Antwerpen, 1975 (Plenum, New York, 1976), **B17**, p. 3.

[46] Y. Meir and N. S. Wingreen, Phys. Rev. **B49**, 11040 (1994).

[47] M. H. Hettler, J. Kroha and S. Hershfield, Phys. Rev. Lett., **73** 1967 (1994).

[48] M. H. Hettler and H. Schöller, Phys. Rev. Lett. **74** 4907 (1995).

[49] S. Hershfield, J. H. Davies and J. W. Wilkins, Phys. Rev. Lett. **67**, 3270 (1991).

[50] Y. Meir and N. S. Wingreen, Phys. Rev. Lett. **68**, 2512 (1992).

[51] J. Annett, N. Goldenfeld, and A. Leggett, LANL cond-mat/9601060 and D.J. Scalapino, Physics Reports **250**, 329 (1995).

[52] Z. X. Shen and D. S. Dessau , Phys. Rep. **253**, 1 (1995).

[53] P. W. Anderson, J. Phys. Chem. Solids **11**, 26 (1959).

[54] L. P. Gor'kov and P. A. Kalugin, Pis'ma Zh. Eksp. Teor. Fiz. **41**, 208 (1985) [JETP Lett. **41**, 253 (1985)].

[55] K. Ueda and T. M. Rice in *Theory of Heavy Fermions and Valence Fluctuations*, eds. T. Kasuya and T. Saso, Springer Series in Solid State Sciences, vol. 62, p. 267 (1985).

[56] K. Ziegler, M. H. Hettler and P. J. Hirschfeld, Phys. Rev. Lett. **77**, 3013 (1996).

[57] P. J. Hirschfeld, D. Vollhardt and P. Wölfle, Sol. St. Commun. **59**, 111 (1986).

[58] S. Schmitt-Rink, K. Miyake and C. M. Varma, Phys. Rev. Lett. **57**, 2575 (1986).

[59] P. J. Hirschfeld, W. O. Putikka, and D. J. Scalapino, Phys. Rev. **B50**, 10250 (1994).

[60] F. Gross, B. S. Chandrasekhar, D. Einzel, K. Andres, P. J. Hirschfeld, H. R. Ott, J. Beuers, Z. Fisk and J. L. Smith, Z. Phys. **B64**, 175 (1986).

[61] Y. Kitaoka, K. Ishida and K. Asayama, J. Phys. Soc. Japan **63**, 2052 (1994).

[62] J. W. Loram, K. A. Mirza, J. R. Cooper and W. Y. Liang, Phys. Rev. Lett. **71**, 1740 (1993).

[63] K. A. Moler, D. J. Baar, J. S. Urbach, R. Liang, W. N. Hardy and A. Kapitulnik, Phys. Rev. Lett. **73**, 2744 (1994); J. of Superconductivity, Vol. 8, No. 1 (1995).

[64] D. A. Bonn, S. Kamal, K. Zhang, R. Liang, D. J. Baar, E. Klein and W. N. Hardy, Phys. Rev. **B50**, 4051 (1994).

[65] J. Giapintzakis, D. M. Ginsberg, M. A. Kirk and S. Ockers, Phys. Rev. **B50**, 15967 (1994).

[66] J. Bardeen, L. N. Cooper and J. R. Schrieffer, Phys. Rev. **108**, 1175 (1957).

[67] A. A. Nersesyan, A. M. Tsvelik and F. Wenger, Phys. Rev. Lett. **72**, 2628 (1994); Nucl. Phys. **B438**, 561 (1995).

[68] D. A. Wollmann, D. J. Van Harlingen, W. C. Lee, D. M. Ginsberg and A. J. Leggett , Phys. Rev. Lett. **71**, 2134 (1993).

[69] D. A. Brawner and H. R. Ott, Phys. Rev. **B49**, 12388 (1994).

[70] C. C. Tsuei, J. R. Kirtley, C. C. Chi, L. S. Yu-Jahnes, A. Gupta, T. Shaw, J. Z. Sun and M. B. Ketchen, Phys. Rev. Lett. **73**, 593 (1994).

[71] J. H. Miller Jr., Q. Y. Ying, Z. G. Zou, N. Q. Fan, J. H. Xu, M. F. Davis and J. C. Wolfe, Phys. Rev. Lett. **74**, 2347 (1995).

[72] G. E. Volovik, Pis'ma ZhETF **58**, 457 (1993); [JETP Lett. **58**, 469 (1993)].

[73] A. A. Abrikosov and L. P. Gor'kov, Soviet Phys. JETP **9**, 220 (1959).

[74] G. M. Eliashberg, Soviet Phys. JETP **11**, 696 (1960).

[75] Y. Nambu, Phys. Rev. **117**, 648 (1960).

[76] V. Ambegoakar, p. 259 *The Green function method*, in R. D. Parks, ed., *Superconductivity* Vol. II, Marcel Dekker, Inc., New York (1969).

[77] N. D. Mermin and H. Wagner, Phys. Rev. Lett. **17**, 1133 (1966).

[78] P. A. Lee and T. V. Ramakrishnan, Rev. Mod. Phys. **57**, 287 (1985).

[79] K. Ziegler, Phys. Rev. **B53**, 9653 (1996).

[80] K. Ziegler, Comm. Math. Phys. **120**, 177 (1988).

[81] J. Annett and N. Goldenfeld, J. Low Temp. Phys. **89**, 197 (1992).

[82] T. Xiang and J.M. Wheatley, Phys. Rev. **B51**, 11721 (1995).

[83] K. Ziegler, Phys. Rev. Lett. **73**, 3488 (1994).

[84] C. Mudry, C. Chamon and X.-G. Wen, Nucl. Phys. **B466**, 534 (1996).

[85] A. L. Fetter, Phys. Rev. **140** A 1921 (1965).

[86] H. Shiba, Prog. Theor. Phys. **40**, 435 (1968).

[87] A. I. Rusinov, Soviet Phys. JETP, **29**, 1101 (1969).

[88] P. Schlottmann, Phys. Rev. **B13**, 1 (1976).

[89] M. Franz, C. Callin and A. J. Berlinsky, Phys. Rev. **B54**, R6897 (1996).

[90] C. H. Choi, Phys. Rev. **B50**, 3491 (1994).

[91] C. H. Choi and P. Muzikar, Phys. Rev. **B41**, 1812 (1990).

[92] A. I. Larkin and Y. N. Ovchinnikov, Soviet Phys. JETP **28**, 1204 (1968).

[93] P. J. Hirschfeld, P. Wölfle and D. Einzel, Phys. Rev. **37**, 83 (1988).

[94] P. J. Hirschfeld, W. O. Putikka, P. Wölfle and Y. Campbell, J. Low Temp. Phys. 88, 395 (1992).

[95] P. A. Lee, Phys. Rev. Lett. **71**, 1887 (1993).

APPENDIX A
ENFORCING THE CONSTRAINT

During the iteration procedure the lesser function can change quite dramatically if the bias and/or temperature is changed substantially. It is not obvious that these changes lead to functions that still fulfill the constraint

$$Z = \int d\epsilon [Na(\epsilon) + Mb(\epsilon)] = 1 \ . \tag{A.1}$$

I would like to enforce the constraint without disturbing the result of the iteration. It does not matter whether I modify the algorithm during the iterations, as long as the modifications vanish when convergence is achieved. I introduce a constant λ_o in a way that allows me to satisfy the constraint after each iteration. Defining

$$a_{\lambda_o}(\omega) = \frac{\Sigma^<(\omega)}{(\omega - \epsilon_d + \lambda_o - \mathrm{Re}\Sigma^r(\omega))^2 + (\mathrm{Im}\Sigma^r(\omega))^2} \tag{A.2}$$

$$b_{\lambda_o}(\omega) = \frac{\Pi^<(\omega)}{(\omega + \lambda_o - \mathrm{Re}\Pi^r(\omega))^2 + (\mathrm{Im}\Pi^r(\omega))^2} \tag{A.3}$$

I determine λ_o by the requirement of fulfilling the constraint

$$\int d\epsilon [Na_{\lambda_o}(\epsilon) + Mb_{\lambda_o}(\epsilon)] = 1 \ . \tag{A.4}$$

A solution can be found by standard methods since the integral is a monotonically

decreasing function of λ_o. After finding λ_o I define new spectral functions via

$$A_{\lambda_o}(\omega) = \frac{\mathrm{Im}\Sigma^r(\omega)}{(\omega - \epsilon_d + \lambda_o - \mathrm{Re}\Sigma^r(\omega))^2 + (\mathrm{Im}\Sigma^r(\omega))^2} \tag{A.5}$$

$$B_{\lambda_o}(\omega) = \frac{\mathrm{Im}\Pi^r(\omega)}{(\omega + \lambda_o - \mathrm{Re}\Pi^r(\omega))^2 + (\mathrm{Im}\Pi^r(\omega))^2} \ . \tag{A.6}$$

I then use these four functions as input for the next iteration. Observe that if I introduced λ_o also in the arguments of the self energies, I would just have shifted the energy scale by λ_o. In that case λ_o would be a modification of the chemical potential μ. During the iterations, when the functions and λ_o are constantly changing, the introduction of λ_o is a significant modification of the 'true' spectral functions. However, as one approaches convergence the changes in the lesser and spectral functions become smaller and smaller, and so are the changes in λ_o. At the point of convergence the changes are negligible and I arrive at functions that are solutions to the NCA–equations and fulfill the constraint. The iteration procedure incorporated λ_o into the solutions, so that at convergence λ_o is indeed just a shift in the energy scale, though it was originally introduced rather artificially to enforce the constraint.

It turns out that the shift due to λ_o has another effect that is quite important for the numerical procedure. As will be explained in more detail in Appendix B it is crucial to use meshes that provide high resolution of all sharp features of the integrand. The lesser and spectral functions have sharp peaks which would shift during the iteration procedure. Thus, one would have to modify the mesh and interpolate the functions after each iteration. However, the changing λ_o com-

pensates these shifts and allows me to work with a fixed mesh. This saves a considerable amount of CPU-time, which is partially the reason why I can reach much lower temperatures than previously obtained.

APPENDIX B

INTEGRATION MESHES FOR EQUILIBRIUM AND NONEQUILIBRIUM NCA

In principle, the integrals in the NCA–equations run from $-\infty$ to ∞ since I am using a gaussian density of states. The smallest features of the integrands have a width given by the temperature T which can be of the order 10^{-7} in terms of the width of the gaussian. Therefore, a linear (equidistant) integration mesh with spacing of about T is out of the question; it would be too time consuming. However, there are only few features of that width whereas most of the integrand has structure on a scale determined by bare level width Γ. So I need to construct a mesh that achieves the resolution of all small scale features like the spectral function peaks and the Fermi (distribution) function step(s) without wasting lots of mesh points in regions where the resolution can be much more coarse.

In equilibrium, this can be achieved by defining the mesh spacing far from the Fermi level ($\epsilon_F = 0$) according to a inverse tangent-function up to an interface point ω_I. There it is matched with a logarithmic mesh that leads up to the Fermi level. In principle, this is nothing but a transformation of the integration variable which I choose corresponding to my needs in different regions of the frequency–axis. Consider L equidistant meshes $\{x_i^l\}$, $i = 1 \ldots n_l$ of n_l, $l = 1 \ldots L$ points. I map these meshes to nonuniform meshes $\{\omega_i^l\}$ via functions $h^l(x^l)$:

$$\omega_i^l = h^l(x_i^l), \quad i = 1 \ldots n^l \tag{B.1}$$

$$\Delta\omega_i^l = \frac{\partial h^l(x_i^l)}{\partial x^l}\Delta x^l \tag{B.2}$$

Here, Δx^l are the spacings of the equidistant meshes. I can now rewrite the numerical integration of an arbitrary function $k(\omega)$ over the nonuniform meshes $\{\omega_i^l\}$ as an integration over the equidistant meshes $\{x_i^l\}$:

$$\begin{aligned}
\textstyle\int_{-\infty}^{\infty} d\omega k(\omega) = \sum_l \int_{a_l}^{b_l} d\omega^l k(\omega^l) \\
\sim \textstyle\sum_l \left(\sum_{i=1}^{n_l-1} \frac{\Delta\omega_i^l}{2}[k(\omega_{i+1}^l) + k(\omega_i^l)] + \frac{1}{2}(k(\omega_1^l)\Delta\omega_1^l + k(\omega_{n_l}^l)\Delta\omega_{n_l}^l)\right) \\
\sim \textstyle\sum_l \left(\frac{\Delta x^l}{2}\sum_{i=1}^{n_l-1}\left[\frac{\partial h^l(x_{i+1}^l)}{\partial x^l}k(x_{i+1}^l) + \frac{\partial h^l(x_i^l)}{\partial x^l}k(x_i^l)\right]\right. \\
\left. + \textstyle\frac{\partial h^l(x_1^l)}{\partial x^l}k(x_1^l) + \frac{\partial h^l(x_{n_l}^l)}{\partial x^l}k(x_{n_l}^l)\right) .
\end{aligned} \tag{B.3}$$

The $a^l = \omega_1^l, b^l = \omega_{n_l}^l$ are the limits of integration of the different regions of the frequency–axis . To cover the whole axis I must have $a^{l+1} = b^l$. In equilibrium, I can get by with four regions: $[-\infty, -\omega_I)$, $[-\omega_I, 0 = \epsilon_F)$, $[0, \omega_I)$, $[\omega_I, \infty]$, where ω_I is an interface frequency ($|\epsilon_d| - \Gamma > \omega_I >> T_K$). If I choose the functions $h^l(x^l)$ as $\tan(x^l)$ in the regions with large absolute frequency and as $\exp(x^l)$ in the regions $|\omega| < \omega_I$ I can create large mesh point spacings far from ϵ_F and exponentially small spacings ('logarithmic' mesh) at $\epsilon_F = 0$. Proper adjustments of constants in the h^l's is required to ensure a smooth crossover of the mesh point spacing at the interface points and a minimal spacing at ϵ_F of at least 10 times smaller than T (and/or V out of equilibrium).

Crucial for the success of this procedure is the introduction of λ_o (see Appendix A) in the iteration procedure. λ_o shifts the peaks of the spectral functions

to the neighborhood of ϵ_F *and keeps them there at every iteration.* Without λ_o the peak positions would shift. So even if I started out with good resolution of the peaks the iteration procedure would move them to regions with worse resolution. This would force me to adjust the integration mesh after each iteration and interpolate the functions on the new mesh at great computational cost in order to keep the resolution. Thus, the introduction of λ_o kills two birds with one stone: It enforces the constraint *and* allows good resolution of all features without changing the integration mesh after every iteration.

Out of equilibrium the distribution function is a double step function with steps at $\pm V/2$. It turns out that (in the Kondo limit) the slave boson spectral and lesser functions show (broadened) peaks at about the same frequencies. However, the pseudofermion functions do not behave as nicely. They do **not** split, but have a single peak somewhere between the Fermi level and $V/2$ that shifts not linearly with V. To cope with such behavior I wish to have good resolution at $\pm V/2$ and at ϵ_F. The latter one is to improve the resolution at the location of the peak of the pseudofermion functions. Unfortunately, I do not know how this location will move with increasing V.

To achieve good resolution at the mentioned frequencies I let the logarithmic mesh end at $\pm V/2$ (coming from larger/smaller frequencies) and choose the spacing in between according to the sum of two tanh–functions which have their zero shifted to $\pm V/4$, respectively. I have to choose parameters of these functions, so that the mesh spacings at the crucial energies is small enough to resolve all features of the integrand. These parameters depend on the bias V. They have

to be calculated before the mesh is 'set up' whenever I change the potential from one run to the next. However, once the mesh is set I do not have to change it anymore during the iteration, because of the same reasons as in equilibrium.

The minimal number of integration points is 200 and 250 for equilibrium and out of equilibrium, respectively. Out of equilibrium I need about 50 points more for the 'inner' region between $\pm V/2$ at moderate bias $V < 20T_K$. For higher bias I have to introduce more points in the inner region. Convergence is achieved within 100 - 200 iterations. The total running time on a current workstation is less than 5 minutes for equilibrium and about 10 minutes out of equilibrium.

APPENDIX C
q–DEPENDENT ORDER PARAMETER PERTURBATIONS TO FIRST ORDER

Here, I compute the q–dependence of small order parameter perturbations $\delta_d(q)$ in a d–wave SC. I use the gap equation with first order self–consistency with respect to $\delta_d(q)$. Furthermore, I assume that q is small compared to the Fermi momentum k_F. Then all important q–dependence comes from the ξ–part of the bulk Green functions (not from Δ_k) I obtain in straightforward generalization of the procedure outlined in Chapter 12

$$\delta_d(q)\left(1/V + TN_o\sum_\omega \int \frac{d\phi}{2\pi}\mathrm{Cos}^2(2\phi)\ \left[(\Delta_\phi^2 - \omega^2 + \frac{1}{4}(\vec{v}_F\vec{q})^2)I_1(\phi) - I_2(\phi)\right]\right)$$
$$= -TN_o\sum_\omega \int \frac{d\phi}{2\pi}\mathrm{Cos}^2(2\phi)\frac{f_o^2 g_o}{1-(f_o g_o)^2}\Delta i\omega I_1(\phi)\,, \tag{C.1}$$

where the integrals $I_1(\phi), I_2(\phi)$ are given by

$$I_1(\phi) = \int d\xi \frac{1}{(\omega^2+\Delta_\phi^2+(\xi+\frac{1}{2}\vec{v}_F\vec{q})^2)(\omega^2+\Delta_\phi^2+(\xi-\frac{1}{2}\vec{v}_F\vec{q})^2)} \tag{C.2}$$
$$I_2(\phi) = \int d\xi \frac{\xi^2}{(\omega^2+\Delta_\phi^2+(\xi+\frac{1}{2}\vec{v}_F\vec{q})^2)(\omega^2+\Delta_\phi^2+(\xi-\frac{1}{2}\vec{v}_F\vec{q})^2)} \tag{C.3}$$

Here, I also ignored all q–dependence which would arise from a nonlinear band about the Fermi level. This is justified for small q and the Fermi energy not to

close to the band edge. The ξ integrals can be performed and give

$$I_1(\phi) = \frac{\pi}{2(\omega^2+\Delta_\phi^2)^{1/2}} \frac{1}{\omega^2+\Delta_\phi^2+\frac{1}{4}(\vec{v}_F\vec{q})^2} \tag{C.4}$$

$$I_2(\phi) = \frac{\pi}{2(\omega^2+\Delta_\phi^2)^{1/2}} \tag{C.5}$$

As for the $q=0$ case I can eliminate the $1/V$–term in Eq. C.1. The final equation for $\delta_d(q)$ reads

$$\begin{aligned} &\delta_d(q)\, T\sum_\omega \int \frac{d\phi}{2\pi} \mathrm{Cos}^2(2\phi) \frac{\Delta_\phi^2+\frac{1}{4}(\vec{v}_F\vec{q})^2)}{(\omega^2+\Delta_\phi^2)^{1/2}} \frac{1}{\omega^2+\Delta_\phi^2+\frac{1}{4}(\vec{v}_F\vec{q})^2} \\ &= -T\sum_\omega \int \frac{d\phi}{2\pi} \mathrm{Cos}^2(2\phi) \frac{f_o^2 g_o}{1-(f_o g_o)^2} \frac{\Delta i\omega}{(\omega^2+\Delta_\phi^2)^{1/2}} \frac{1}{\omega^2+\Delta_\phi^2+\frac{1}{4}(\vec{v}_F\vec{q})^2} \end{aligned} \tag{C.6}$$

A similar result was previously derived by Choi [90] by means of a quasi–classical approximation. However, his result has either a misprint or is only valid in the Ginzburg–Landau regime, i.e. in the case of a small order parameter Δ_ϕ. The above result is valid for all temperatures under the above mentioned conditions.

BIOGRAPHICAL SKETCH

I was born on the 13th of August, 1966, as youngest child to my parents Heinrich Hettler and Maria Hettler in the town of Bühl/Baden in the Federal Republic of Germany. I entered elementary school in 1972 and graduated from the grammar school Windeck–Gymnasium in Bühl/Baden in May 1985. From October 1985 to December 1986 I did mandatory service in the german army.

In October 1986 I entered the Universität Karlsruhe at Karlsruhe, Germany, as a student of physics. I graduated in 1992 with the Diplom in physics, an equivalent to the master's degree. In August 1992 I entered the doctoral program in physics at the University of Florida in Gainesville, Florida. I will graduate with the Ph.D. degree in physics in December 1996.

I certify that I have read this study and that in my opinion it conforms to acceptable standards of scholarly presentation and is fully adequate, in scope and quality, as a dissertation for the degree of Doctor of Philosophy.

Peter J. Hirschfeld, Chair
Associate Professor of Physics

I certify that I have read this study and that in my opinion it conforms to acceptable standards of scholarly presentation and is fully adequate, in scope and quality, as a dissertation for the degree of Doctor of Philosophy.

Selman Hershfield
Assistant Professor of Physics

I certify that I have read this study and that in my opinion it conforms to acceptable standards of scholarly presentation and is fully adequate, in scope and quality, as a dissertation for the degree of Doctor of Philosophy.

Khandker A. Muttalib
Associate Professor of Physics

I certify that I have read this study and that in my opinion it conforms to acceptable standards of scholarly presentation and is fully adequate, in scope and quality, as a dissertation for the degree of Doctor of Philosophy.

David Tanner
Professor of Physics

I certify that I have read this study and that in my opinion it conforms to acceptable standards of scholarly presentation and is fully adequate, in scope and quality, as a dissertation for the degree of Doctor of Philosophy.

Joseph H. Simmons
Professor of Materials Science and Engineering

This dissertation was submitted to the Graduate Faculty of the Department of Physics in the College of Liberal Arts and Sciences and to the Graduate School and was accepted as partial fulfillment of the requirements for the degree of Doctor of Philosophy.

December 1996

Dean, Graduate school